Female-germline specific protein Sakura interacts with Otu and is crucial for germline stem cell renewal and differentiation and oogenesis

Azali Azlan[1], Li Zhu[1], and Ryuya Fukunaga[1*]

[1]*Department of Biological Chemistry, Johns Hopkins School of Medicine, Baltimore, MD 21205*

*Corresponding author

Email: (fukunaga@jhmi.edu)

Abstract

During oogenesis, self-renewal and differentiation of germline stem cells (GSCs) must be tightly regulated. The *Drosophila* female germline serves as an excellent model for studying these regulatory mechanisms. Here, we report that a previously uncharacterized gene *CG14545*, which we named *sakura*, is essential for oogenesis and female fertility in *Drosophila*. Sakura is predominantly expressed in the ovaries, particularly in the germline cells, including GSCs. *sakura* null mutant female flies display rudimentary ovaries with germline-less and tumorous phenotypes, fail to produce eggs, and are completely sterile. The germline-specific depletion of *sakura* impairs Dpp/BMP signaling, leading to aberrant *bag-of-marbles* (*bam*) expression, resulting in faulty differentiation and loss of GSCs. Additionally, *sakura* is necessary for normal piwi-interacting RNAs (piRNAs) levels and for proper localization of Oo18 RNA-binding protein (Orb) in developing oocytes. We identified Ovarian Tumor (Otu) as protein binding partner of Sakura, and we found that loss of *otu* phenocopies loss of *sakura* in ovaries. Thus, we identified Sakura as a

21 crucial factor for GSC renewal and differentiation and oogenesis, and propose that Sakura and Otu

22 function together in these processes.

Introduction

Oogenesis is a complex process in which germline stem cells (GSCs) develop into mature female gametes or oocytes. This process involves multiple layers of regulations and numerous genes, some of which remain to be discovered and characterized. *Drosophila melanogaster*, a genetically tractable model organism, has long been at the forefront of oogenesis research.

Adult *Drosophila* females possess a pair of ovaries, each composed of 12-16 ovarioles. At the anterior tip of each ovariole is a structure called the germarium, which houses two to three GSCs (Fig S1). GSCs reside in the most anterior region of the germarium, where they directly contact cap cells and escort cells, forming a niche crucial for GSC self-renewal [1–3]. GSCs undergo asymmetric mitotic division, producing two distinct cells: one GSC and one cystoblast[1,4]. The cystoblast, destined to differentiate, undergoes four mitotic divisions with incomplete cytokinesis, resulting in interconnected cysts of 2, 4, 8, and 16 cells [5,6]. Of the 16 cells, one will differentiate into an oocyte, while the remaining 15 develop into polyploid nurse cells, which synthesize proteins and RNAs for deposition into the oocyte[7].

GSC proliferation is essential for proper oogenesis. GSCs must be tightly regulated to maintain their undifferentiated state while continuing to divide and differentiate. Failure in GSC self-renewal or inappropriate differentiation leads to stem cell loss, disrupting oocyte production[8,9]. Conversely, uncontrolled GSC division or defective differentiation results in an overabundance of GSC-like cells (a tumorous phenotype) and fewer differentiated cells, ultimately inhibiting oocyte production[10,11]. Thus, a precise balance between GSC self-renewal and cyst differentiation within the germarium is essential for proper oogenesis and is tightly regulated.

Bone Morphogenetic Protein (BMP) signaling plays a critical role in regulating GSC self-renewal and differentiation during *Drosophila* oogenesis. In the stem cell niche, GSCs are physically anchored to cap cells via adherens and gap junctions[12,13]. Cap cells secrete BMP ligands, such as Decapentaplegic (Dpp) and Glass bottom boat (Gbb), which are recognized by transducing receptors like Thickvein (Tkv) and Saxophone (Sax) on the GSCs[14,15] (Fig S1). Upon activation, these receptors phosphorylate a transcription factor Mad. The phosphorylated Mad (pMad) translocates into the nucleus, where it represses the transcription of *bag-of-marbles* (*bam*), a key differentiation factor [16,17].

Bam, a ubiquitin-associated protein, is essential for cystoblast differentiation. Dpp/BMP signaling in the niche represses *bam* expression, preventing GSCs from differentiating and enabling self-renew. However, as the daughter cells (cytoblasts) exit the niche, they derepress *bam* and initiate the differentiation program (Fig S1)[7]. Tight regulation of Dpp/BMP signaling and *bam* expression ensures that only cells within the niche adopt GSC fate, while adjacent daughter cells differentiate into cystoblasts. Loss of *bam* leads to blocked differentiation and the accumulation of GSC-like cells, whereas ectopic *bam* expression forces GSCs differentiation, depleting the stem cell pool [18–20].

One of the proteins that interacts with Bam is Ovarian Tumor (Otu). Otu forms a deubiquitinase complex with Bam, which deubiquitinates Cyclin A (CycA), stabilizing CycA and promoting GSC differentiation[21]. Otu is crucial for oogenesis and female fertility[22,23]. Mutations in the *otu* gene cause various ovarian defects, including tumorous growths, germ cell loss, and abnormalities in oocyte determination and nurse cell dumping, indicating Otu's importance in multiple stages of oogenesis[22–25]. However, the precise molecular mechanisms by which Otu functions in these processes remain largely unknown.

In this study, we aimed to identify a novel gene required for oogenesis. Through a search for uncharacterized genes expressed exclusively in *Drosophila* ovaries, we discovered *CG14545*, a gene encoding a 114 amino acids (aa) long protein without any known functional domain (Fig 1A). CG14545 is expressed specifically in female germline cells, including GSCs. Our genetic analysis revealed that *CG14545* is required for oogenesis and female fertility and plays an important intrinsic role in regulating GSCs renewal and differentiation. Additionally, CG14545 is important for the piRNA pathway. We identified Otu as a binding partner of the CG14545 protein, suggesting that both proteins may participate in the same molecular pathways to regulate GSC fate and differentiation. We named the *CG14545* gene *sakura*, meaning "cherry blossom" in Japanese, symbolizing birth and renewal.

Results

Sakura is exclusively expressed in the ovaries

Based on high-throughput expression data in Flybase, *sakura* mRNA is highly and exclusively expressed in adult ovaries (Fig 1B). To investigate Sakura protein expression, we generated a polyclonal anti-Sakura antibody against a recombinant full-length Sakura protein. Using this antibody, we examine Sakura protein expression at different stages of *Drosophila* development and across tissues. We found that Sakura protein is specifically expressed in the ovary, particularly in stage 1-11 oocytes (Fig 1C).

88 ***sakura* mutant flies**

89 To explore the biological and molecular functions of Sakura *in vivo*, we generated a *sakura* mutant
90 allele (*sakura*^{null}) with a one nucleotide (nt) insertion replacing 33 nts within the Sakura coding
91 region using the CRISPR/Cas9 genome editing system (Fig 1A)[26]. This mutation causes a
92 frameshift and a premature stop codon, resulting in a 33-amino acid (aa) N-terminal fragment of
93 Sakura followed by a 22-aa segment produced by frameshifted translation (Fig 1A). This truncated
94 fragment is unlikely to be functional, and we were unable to detect stable protein expression, as
95 shown below. Thus, we consider this allele a null mutation. *sakura*$^{null/null}$ flies were viable,
96 revealing that Sakura is not essential for survival.

97 To validate the *sakura*^{null} strain, we performed Western blots using ovary lysates from
98 *sakura* mutant flies using the anti-Sakura antibody. As expected, full-length Sakura protein was
99 detected in the ovaries of wild-type (*sakura*$^{+/+}$) and heterozygous controls (*sakura*$^{null/+}$), but not in
100 those of homozygous mutants (*sakura*$^{null/null}$) (Fig 1D). No smaller protein corresponding to the
101 truncated Sakura fragment was detected in either *sakura*$^{null/+}$ or *sakura*$^{null/null}$ ovaries thus,
102 suggesting that the fragment is unstable or not expressed.

103

104 **Sakura is cytoplasmic and expressed specifically in germ cells**

105 To determine the localization of Sakura protein within the ovaries, we generated transgenic flies
106 carrying a *sakura* coding sequence fused with EGFP at the C-terminus (*sakura*-EGFP) under the
107 control of the *sakura* promoter. Western blot analysis of ovary lysates showed that Sakura-EGFP
108 is expressed at levels comparable to endogenous Sakura (Fig 1D). Confocal imaging revealed that
109 Sakura-EGFP is specifically expressed in the cytoplasm of germ cells, including GSCs, cyst cells,

110 nurse cells, and developing oocytes (Fig 1E and 1F). Sakura-EGFP was not expressed in somatic
111 cells such as terminal filament, cap cells, escort cells, or follicle cells. (Fig 1E). In the egg chamber,
112 Sakura-EGFP was detected in the cytoplasm of nurse cells and was enriched in developing oocytes
113 (Fig 1F).

114

115 ***sakura* is essential for female fertility**

116 Given its ovary-specific expression at both mRNA and protein levels (Fig 1B and 1C), we
117 hypothesized that Sakura plays a critical role in ovarian function. Fertility assays revealed that
118 *sakura*$^{null/null}$ females laid no eggs when mated with wild-type males, while control female flies
119 (*sakura*$^{+/+}$ and *sakura*$^{null/+}$) laid numerous eggs (Fig 2A). Dissection of *sakura*$^{null/null}$ ovaries
120 revealed that they were rudimentary compared to normal ovaries in controls (Fig 2C). This
121 suggests that the inability of *sakura*$^{null/null}$ female to lay eggs is due to their underdeveloped ovaries.
122 In contrast, *sakura*$^{null/null}$ males were fertile and showed no significant differences compared to
123 controls (*sakura*$^{+/+}$ and *sakura*$^{null/+}$) (Fig S2).

124 To confirm that the observed female sterility was caused by the loss of *sakura*, we
125 generated *sakura* rescue flies expressing Sakura-EGFP in the *sakura*$^{null/null}$ background
126 (*sakura*$^{null/null}$; *sakura-EGFP*). Western blotting confirmed that these flies expressed Sakura-EGFP,
127 but not endogenous Sakura (Fig 1D). The *sakura-EGFP* transgene fully rescued both female
128 fertility and ovary morphology in the *sakura*$^{null/null}$ background (Fig 2). *sakura-EGFP* rescue
129 females showed no significant fertility differences compared to controls (Fig 2A and 2B), and their
130 ovaries were normal in shape and size (Fig 2C). We concluded that Sakura is essential for female

131 fertility and normal ovary morphology but dispensable for male fertility, consistent with the
132 observation that Sakura is predominantly expressed in ovarian germline cells (Fig 1).

133

134 **$sakura^{null/null}$ ovaries are germless and tumorous**

135 Given the rudimentary appearance of $sakura^{null/null}$ ovaries, we questioned whether they contained
136 germ cells. We used flies carrying *vasa-EGFP* knocked-in reporter in the $sakura^{null/null}$ background,
137 as Vasa is a known germ cell marker[7]. We observed that some $sakura^{null/null}$ ovarioles were devoid
138 of germ cells ("germless"), while others retained germ cells (Fig 3A), suggesting that loss of *sakura*
139 leads to germ cell depletion. Additionally, $sakura^{null/null}$ ovaries exhibited significantly higher
140 levels of cleaved Caspase-3 staining, indicative of apoptosis, compared to controls ($sakura^{null/+}$)
141 (Fig 3B).

142 Oogenesis begins in the germarium, which contains 2-3 GSCs identified by round,
143 unbranched spectrosomes that contact cap cells[7] (Fig S1). In contrast, cysts have branched
144 fusomes. Immunostaining with hu-li tai shao (HTS) antibody, which marks spectrosomes and
145 fusomes, revealed an excess number of GSC-like cells with round spectrosomes in $sakura^{null/null}$
146 ovarioles containing germ cells (Fig 3C, red stars), indicative of a "tumorous" phenotype as
147 previously described[27–29]. Additionally, we observed an excess number of cyst cells with branched
148 fusomes that persisted throughout the ovarioles (Fig 3C), suggesting abnormal cyst cell
149 differentiation and division.

150 Within the same ovary, some $sakura^{null/null}$ ovarioles exhibited the tumorous phenotype,
151 while others were germless, without any spectrosome or fusome staining (Fig 3C, green stars).
152 Quantification revealed that 35% of $sakura^{null/null}$ ovarioles were tumorous while the remaining

153 65% were germless (n=74) (Fig 3D). In contrast, no tumorous or germless phenotypes were
154 observed in control (*sakura*$^{+/+}$ and *sakura*$^{null/+}$) or *sakura-EGFP* rescue flies (Fig 3D).
155 Furthermore, ~95% of *sakura*$^{null/null}$ ovarioles with germ cells contained excess GSC-like cells (>5)
156 (Fig 3E and Fig S3). The mean number of GSCs or GSC-like cells for *sakura*$^{+/+}$, *sakura*$^{null/+}$, and
157 *sakura-EGFP* rescue was 2.2 ± 0.6, 2.2 ± 0.6, and 2.1 ± 0.7, respectively while that for *sakura*$^{null/null}$
158 was 26.5 ± 17.5 (p-value <0.05). These results suggest that Sakura is essential for regulating GSC
159 division and differentiation. Overall, we conclude that Sakura is required for germ cell survival,
160 division, and differentiation.

161

162 **Loss of *sakura* results in reduced germline piRNA**

163 Piwi-interacting RNAs (piRNAs) are produced in germline cells and somatic follicle cells and
164 transcriptionally and post-transcriptionally silence transposon expression through sequence-
165 complementarity. Disruption of the piRNA pathway can result in oogenesis arrest, germ cell loss,
166 rudimentary ovaries, and sterility[9,30]. Loss of piRNAs in germ cells leads to the upregulation
167 (desilencing) of transposons, increased DNA damage, and apoptotic cell death[31]. We investigated
168 whether the loss of *sakura* would result in loss of piRNA and transposon upregulation. We
169 performed high-throughput sequencing (small RNA-seq and polyA+ RNA-seq) on ovary RNA
170 samples from *sakura*$^{+/+}$, *sakura*$^{null/+}$, *sakura*$^{null/null}$, and *sakura-EGFP* rescue (*sakura*$^{null/null}$ with
171 *sakura-EGFP*) flies.

172 piRNA levels in *sakura*$^{null/null}$ ovaries were reduced compared to controls (*sakura*$^{+/+}$), while
173 *sakura*$^{null/+}$ and *sakura-EGFP* rescue showed no such reduction (Fig 4A). Consistent with this,
174 transposon RNA levels in *sakura*$^{null/null}$ ovaries were upregulated compared to *sakura*$^{+/+}$, while

175 *sakura*$^{null/+}$ and *sakura-EGFP* rescue showed no such upregulation (Fig 4B). Given that Sakura is
176 specifically expressed in germline cells, but not in somatic cells (Fig 1E and 1F), we hypothesized
177 that loss of *sakura* interrupts the piRNA pathway in germ cells, leading to the desilencing of
178 germline transposons. A well-characterized germline transposon in *Drosophila* is *Burdock*[30,32]. We
179 found that *Burdock* piRNA levels were significantly lower in *sakura*$^{null/null}$ compared to controls
180 and rescue flies (Fig 4C).

181 We employed the *Burdock* sensor, a transposon reporter tool to monitor germline piRNA
182 activity[30]. The reporter expresses nuclear GFP and β-gal under the control of the *nanos* promoter
183 for germline expression, with a target sequence for *Burdock* piRNAs in the 3′ UTR[30] (Fig 4D).
184 Using a *sakura* RNAi line driven by *UAS-Dcr2* and *NGT-Gal4* to knock down *sakura* specifically
185 in the germline, we observed that GFP and β-gal expression were highly elevated in *sakura*
186 knockdown germlines compared to control RNAi (y^{RNAi}) knockdowns (Fig 4D). This confirmed
187 that loss of *sakura* leads to a loss of piRNA-mediated transposon silencing in the germline. We
188 conclude that Sakura is essential for proper piRNA levels and piRNA-based transposon silencing
189 in the germline.

190

191 **_sakura_ is important for oogenesis in germline cells beyond GSCs and germline cysts**

192 Both *sakura*$^{null/null}$ and *sakura* germline RNAi knockdown driven by *UAS-Dcr-2* and *NGT-Gal4*,
193 which initiates RNAi in germline from GSCs, resulted in rudimentary ovaries (Fig 2C and 5A).
194 These ovaries lacked later-stage germline cells and egg chambers, making it difficult to assess the
195 role of Sakura beyond the germarium. However, because Sakura-EGFP expression is not limited

196 to GSCs and germline cysts (Fig 1E and 1F), we speculated that Sakura might function in later-
197 stage germline cells as well.

198 To explore this possibility, we used *TOsk-Gal4* (a combination of *osk-Gal4* and *αTub67C-*
199 *Gal4*) to drive *sakura* RNAi knockdown in germline cells after the germline cyst stage (from
200 germarium region 2b onward. Fig S1A), sparing GSCs and germline cysts[33]. Unlike *NGT-Gal4*,
201 *TOsk-Gal4*-driven *sakura* RNAi knockdown did not drastically affect ovary morphology (Fig 5A),
202 allowing us to study the effects of *sakura* loss in egg chambers. We confirmed *sakura* RNAi
203 (*sakura RNAi #1* and #2) knockdown efficiency by Western blot, showing effective depletion of
204 Sakura in ovaries from both *NGT-Gal4* and *TOsk-Gal4*-driven RNAi lines (Fig 5B).

205 Interestingly, *TOsk-Gal4*-driven *sakura* RNAi knockdown severely reduced the numbers
206 of eggs laid (Fig 5C) and stage 14 oocytes in ovaries compared to control RNAi (y^{RNAi}) (Fig 5D),
207 suggesting that *sakura* is important for oogenesis beyond the germline cyst stage. Additionally, we
208 observed mislocalized and dispersed Oo18 RNA-binding protein (Orb. A marker for oocyte
209 identity) in *TOsk-Gal4*-driven *sakura* RNAi knockdowns (Fig 5E). Proper Orb localization is
210 critical for oocyte specification and maintenance[34], and its mislocalization likely underlies the
211 reduced ability to produce stage 14 oocytes and eggs *sakura* knockdown flies (Fig 5C and 5D).
212 We conclude that Sakura is crucial for proper Orb localization and in germline cells beyond GSCs
213 and germline cysts. In subsequent *sakura* RNAi experiments, we used the *sakura RNAi* #2 line.

214

215 **Sakura is required intrinsically for GSC establishment, maintenance, and differentiation**

216 To explore whether *sakura* functions autonomously in the germline, we conducted mosaic analysis
217 using the FLP-FRT system[35]. First, we assessed its role in GSC establishment by marking $sakura^{null}$

218 clones in primordial germ cells (PGCs)) before the early third instar larval stage and tracking their
219 development into adult GSCs, as described in a previous study[36]. In control adult flies,12.3%
220 (20/163) of GSCs were marked, while only 1.9% (4/213) were marked in *sakura*^{null} mutants,
221 demonstrating that *sakura* is autonomously important for GSC establishment.

222 Next, we assessed GSC maintenance by generating marked *sakura*^{null} GSCs in adult flies
223 using the FLP-FRT system and measuring their loss rate over time [14,36]. The percentage of marked
224 control GSC clones and marked *sakura*^{null} GSC clones 4 days after clone induction was 27.8% and
225 22.1%, respectively (Fig 6A). These numbers were considered the initial percentage. The
226 percentage of marked control GSCs decreased to 25.8% and 16.8% on days 7 and 14, respectively
227 (Fig 6A), resulting in a loss rate of 39.4% over the 10-day testing period (from day 4 to day 14).
228 In contrast, the percentage of marked *sakura*^{null} GSC clones decreased to 16.3% and 5.4% on days
229 7 and 14, respectively. Thus, the loss rate of *sakura*^{null} GSCs is 75.6% over the 10-day period,
230 which is higher than controls. We conclude that *sakura* is intrinsically required for GSC
231 maintenance.

232 Germline depletion of *sakura* caused germless and tumorous phenotypes (Fig 3). To
233 determine whether *sakura* is intrinsically required in the germ line cells for GSC differentiation,
234 we quantified the number of marked (GFP-negative) and unmarked (GFP-positive) GSC-like cells
235 (germline cells with a round spectrosome) in the germaria carrying marked GSC clones at 4, 7,
236 and 14 days after clone induction. We found that the number of marked *sakura*^{null} GSC-like cells
237 was higher than that of marked control GSC-like cells at all time points (Fig 6C). The number of
238 marked *sakura*^{null} GSC-like cells increased over the 10-day period, while the number of marked
239 control cells did not (Fig 6C). In contrast, the number of unmarked GSC-like cells in germaria
240 containing *sakura*^{null} GSC clones did not differ significantly from those in germaria containing

241 control GSC clones, and the number did not increase (Fig S4). These results indicate that *sakura*
242 is intrinsically important in germline cells, including GSCs, to regulate their proper division and
243 differentiation. Taken together, we conclude that *sakura* is required intrinsically for GSC
244 establishment, maintenance, and differentiation.

245

246 **Loss of *sakura* inhibits Dpp/BMP signaling**

247 Dpp/BMP signaling is a key pathway regulating GSC self-renewal and differentiation (Fig S1)[7,37].
248 We hypothesized that the germless and tumorous phenotypes observed in *sakura* loss-of-function
249 ovaries could be due to Dpp/BMP signaling misregulation. To test this, we knocked down *sakura*
250 in the germline driven by *UAS-Dcr2* and *NGT-Gal4* in the presence of *bam-GFP* reporter[38]. In
251 controls (y^{RNAi}), Bam-GFP expression was restricted to 8-cell cysts and disappeared in 16-cell cysts
252 and onward (Fig 7A)[38]. However, in *sakura* knockdowns, Bam-GFP expression persisted
253 throughout the ovariole, with excess Bam-GFP positive cells (Fig 7A). This suggests that Bam
254 expression is not repressed by Dpp/BMP signaling, leading to GSC loss in *sakura* knockdowns.

255 To further confirm this finding, we used the FLP-FRT technique to induce $sakura^{null}$ clones
256 in the germaria and stained them with anti-Bam antibody[20]. All $sakura^{null}$ clones expressed Bam
257 throughout the germarium, whereas in control clones, Bam was not expressed in the GSCs and
258 was restricted to cyst cells (Fig 7B). In GSCs, pMad translocates into the nucleus to repress Bam
259 expression [16,17](Fig S1). We stained ovaries with anti-pMad antibodies and found that pMad
260 intensity was significantly reduced in $sakura^{null}$ GSC clones compared to control GSCs (Fig 7C
261 and D). This indicates that the dysregulated Bam expression observed in $sakura^{null}$ was due to
262 reduced pMad levels in GSCs.

263 Previous studies have shown that ectopic expression of a stable form of CyA leads to germ
264 cell loss[39]. This germ cell loss phenotype is also observed upon ectopic *bam* expression in
265 GSCs[14,40,41]. It was reported that Bam associates with Ovarian tumor (Otu) to promote
266 deubiquitination and stabilization of CycA[21]. Since we observed derepressed *bam* expression in
267 *sakura*^{null} cells, we investigated whether CycA levels were affected. Staining ovaries with anti-
268 CycA antibodies revealed higher CycA intensity in *sakura*^{null} clones compared to neighboring
269 wild-type cells in the same germarium and control clones in control germarium (Fig 7E). *sakura*^{null}
270 clones exhibited significantly higher mean CycA intensity compared to control clones (Fig 7F).
271 The elevated CycA levels in *sakura*^{null} clones likely results from Bam misexpression and Bam-
272 mediated stabilization.

273 Finally, we tested whether we could rescue the germless phenotype caused by *sakura* loss-
274 of-function by knocking down either *bam* or *cycA* in the germline. Double RNAi knockdown of
275 *sakura* and *bam* in the germline using *UAS-Dcr-2* and *NGT-Gal4* partially rescued the germless
276 phenotype (Fig 8). In contrast, knocking down *sakura* and *cycA* together failed to rescue the
277 germless phenotype (Fig 8). This suggests that the germless phenotype of *sakura* is partly due to
278 *bam* misexpression, not *cycA*.

279

280 **Sakura binds Otu**

281 To explore the molecular function of Sakura in oogenesis, we aimed to identify Sakura-interacting
282 proteins. We conducted a co-immunoprecipitation experiment using anti-GFP magnetic beads on
283 the ovary lysates of flies expressing Sakura-EGFP, followed by mass spectrometry to identify co-
284 immunoprecipitated proteins. Ovary lysates from flies without the *sakura-EGFP* transgene

285 (*w1118*) served as negative controls. Mass spectrometric analysis revealed several proteins with
286 peptide signals present in all three biological replicates of the Sakura-EGFP samples without any
287 signals in any of the three biological replicates of the negative control (Table 1). Among these, the
288 most promising candidate, exhibiting the highest unique peptide signal in each of three replicates
289 of the Sakura-EGFP samples was Otu.

290 To confirm this finding, we generated a polyclonal anti-Otu antibody. Using Western blot
291 analysis, we detected endogenous Otu protein in the Sakura-EGFP immunoprecipitants from
292 ovaries, but not in the negative control (Fig 9A), validating the mass spectrometry results. Next,
293 using wild-type (without Sakura-EGFP) ovary lysates, we immunoprecipitated endogenous Sakura
294 with anti-Sakura antibody and detected endogenous Otu in the immunoprecipitant by Western blot
295 (Fig 9B), demonstrating that endogenous Sakura interacts with endogenous Otu. Furthermore, we
296 found that ectopically expressed Flag-tagged Otu co-immunoprecipitated with ectopically
297 expressed HA-tagged Sakura in S2 cells (Fig 9C).

298 The *otu* gene encodes two annotated protein isoforms, a predominant 98 kDa isoform and
299 a less abundant 104 kDa isoform resulting from alternative splicing[42]. The 98kDa isoform lacks
300 Tudor domain encoded in an alternatively spliced 126-bp exon[43]. It has been reported that the 104
301 kDa Otu isoform can perform all functions, while the 98 kDa Otu isoform functions in later stages
302 of oogenesis, such as nurse cell regression and oocyte maturation[44]. The major Otu isoform
303 observed in the inputs and immunoprecipitates from ovaries in Figure 9 corresponds to the 98 kDa
304 isoform.

305 Next, we sought to identify which regions of Sakura and Otu are important for their
306 interaction. We predicted the structure of the Sakura-Otu protein complex using AlphaFold[45].
307 AlphaFold suggests that the N-terminal region of Sakura (1-49aa) and the N-terminal region of

308 Otu (1-405aa) are highly likely to form interactions, while the C-terminal region of Sakura (100-
309 144aa) does not interact with Otu (Fig 10A-C). The Tudor domain of Otu is not directly involved
310 in this interaction. To experimentally validate the predictions made by AlphaFold, we generated a
311 series of truncated Otu fragments, including Otu(ΔTudor) (1-336, 389-853aa, corresponding to the
312 endogenous 98 kDa isoform), Otu(N1) (1-405aa), Otu(N2) (1-339aa), and Otu(C) (405-853aa)
313 (Fig 10B). We then performed co-immunoprecipitation assays to test which fragments could
314 interact with full-length Sakura. All fragments except Otu(C) were associated with full-length
315 Sakura protein in S2 cells (Fig 10D), demonstrating that the C-terminal low-complexity region of
316 Otu is dispensable for the interaction. This assay also showed that the Tudor domain is not critical
317 and the N-terminal fragment (1-339aa) of Otu is sufficient for interaction with Sakura. These
318 findings align well with the predictions made by AlphaFold.

319 Subsequently, we created several truncated Sakura fragments and conducted co-
320 immunoprecipitation assays in S2 cells to determine which Sakura fragments can interact with
321 full-length Otu. The fragments generated included Sakura(NM) (1-100aa), Sakura(NC) (1-49, 100-
322 144aa), Sakura(MC) (49-144aa), Sakura(N) (1-49aa), Sakura(M) (49-100aa), and Sakura(C) (100-
323 144aa) (Fig 10C). We found that Sakura(NM), Sakura(NC), Sakura(N), and Sakura(M) were
324 associated with Otu (Fig 10E). Compared to Sakura(NM) and Sakura(N), the interaction of
325 Sakura(M) with Otu is relatively weaker, as indicated by a fainter band in the Western blot (Fig
326 10E). Sakura-NC exhibited a weak interaction with Otu, while Sakura(MC) and Sakura(C) showed
327 no interaction (Fig 10E). These assays demonstrated that the N-terminal region (1-49aa) of Sakura
328 is sufficient for interaction with Otu. Moreover, the results suggest that the C-terminal region of
329 Sakura (100-144aa) does not interact with Otu and that adjoining it with the N-terminal (1-49aa)

330 or the middle (M) region (49-100aa) weakens the interaction with Otu. These findings support the
331 AlphaFold predictions.

332 Finally, to test whether the interaction between Sakura and Otu can be achieved solely
333 through their N-terminal regions, we performed co-immunoprecipitation assay with Sakura(N) and
334 Otu(N2). We discovered that they interact each other (Fig 10F). A reciprocal co-
335 immunoprecipitation assay also confirmed their interaction (Fig S5), revealing that the interaction
336 between Sakura and Otu can be established with just the 1-49aa of Sakura and the 1-339aa of Otu.
337 Therefore, we conclude that Sakura interacts with Otu *in vivo,* and the N-terminal regions of both
338 proteins are sufficient for their interaction.

339

340 **Loss of *otu* phenocopies loss of *sakura***

341 Having established the interaction between Sakura and Otu, we were interested in whether they
342 function together during oogenesis. We speculated that for them to interact and function together,
343 Sakura and Otu must exhibit similar expression and localization patterns in ovaries. We generated
344 two transgenic flies carrying full-length *otu-EGFP* or *otu(ΔTudor)-EGFP* transgenes; both
345 constructs are C-terminally fused with EGFP and under the control of the *otu* promoter. We found
346 that both Otu-EGFP and Otu(ΔTudor)-EGFP display similar expression and localization patterns
347 to Sakura-EGFP (Fig 1E, 1F and Fig 11A). Like Sakura-EGFP, Otu-EGFP and Otu(ΔTudor)-EGFP
348 are specifically expressed in germ cells, but not in follicle cells, and are localized to the cytoplasm,
349 being enriched in the developing oocytes (Fig 11A). We did not observe any difference in
350 localization patterns between Otu-EGFP and Otu(ΔTudor)-EGFP; suggesting that the Tudor

351 domain is not crucial for Otu protein localization. Notably, the localization pattern exhibited by
352 the transgenic Otu-EGFP generated in this study is consistent with a previous report [23].

353 Previous studies have shown that mutations in *otu* lead to severe defects in germ cell
354 division and differentiation, resulting in a tumorous phenotype[22–24,42]. To study the role of *otu*
355 specifically in the germline, we performed RNAi knockdown of *otu* in the germline driven by *nos-*
356 *Gal4-VP16*. Interestingly, we found that germline depletion of *otu* results in rudimentary ovaries,
357 similar to the loss of *sakura* (Fig 2D, Fig 5A, and Fig 11B). Furthermore, similar to *sakura* RNAi
358 (Fig 5)*, TOsk-Gal4*-driven *otu* RNAi knockdown did not affect ovary morphology (Fig 11B), but
359 it did result in a reduced number of eggs laid and stage 14 oocytes compared with control RNAi
360 (w^{RNAi}) (Figure 11C and 11D).

361 When *sakura* and *otu* were independently RNAi-knockdowned in the germline driven by
362 *UAS-Dcr2* and *NGT-Gal4*, the percentages of germless ovaries for *otu-RNAi* and *sakura-RNAi*
363 were similar (~70%) (Fig 8). However, when *otu* and *sakura* were knocked down together, the
364 percentage of germless ovaries increased significantly to 79% (Fig 8), suggesting that the double
365 knockdown of *otu* and *sakura* enhances the germless phenotype in the ovaries.

366 Next, we used the *Burdock* sensor to test if loss of *otu* leads to loss of piRNA-mediated
367 transposon silencing in the germline. Similar to *sakura* (Fig 4D), germline depletion of *otu* resulted
368 in elevated GFP and β-Gal produced by the *Burdock* sensor (Fig 11E), indicating loss of piRNA-
369 mediated transposon silencing. To determine if germ cell loss caused by *otu-RNAi* is a result of
370 apoptosis, we stained the rudimentary ovaries of *otu-RNAi* for cleaved Caspase-3. Similar to
371 $sakura^{null/null}$ (Fig 3B), cleaved Caspase-3 signals were higher in *otu-RNAi* ovaries than in controls,
372 suggesting that the observed germ cell loss is due to apoptosis (Fig 11F).

373 Loss of *sakura* leads to misexpression of *bam,* likely due to low levels of pMad in the germ
374 cells (Fig 7A-C). We were curious whether a similar occurrence could be observed in *otu-RNAi*.
375 In the *otu* germline RNAi knockdown ovaries, we found that Bam-GFP expression is not restricted
376 to the germarium but persists throughout the ovariole, resulting in an excess number of Bam-GFP-
377 positive cells (Fig 12A). We also observed lower pMad levels in $otu^{14/14}$ mutant GSCs (Fig 12B).
378 These data suggest that, similar to *sakura*, loss of *otu* results in *bam* derepression, likely due to
379 low levels of pMad in the germ cells.

380 A previous study has shown that Otu possesses deubiquitinase activity[21]. We asked whether
381 Sakura regulates the Otu's deubiquitinase activity. To test this, we performed an in vitro
382 deubiquitination assay using Ub-Rhodamine 110 as a model substrate. Consistent with previous
383 studies[21], we detected a deubiquitinase activity in Otu that was ectopically expressed and purified
384 from S2 cells (Fig S6). The presence of Sakura, purified from *E.coli,* did not affect Otu's
385 deubiquitinase activity under these assay conditions. Additionally, Sakura itself did not exhibit
386 deubiquitinase activity.

387 Taken together, these findings show that *otu* and *sakura* phenocopy each other in ovaries,
388 specifically in regulating germ cell maintenance and differentiation, raising the possibility that
389 they function together. Similar to *sakura*, loss of *otu* inhibits Dpp/BMP signaling and results in the
390 de-repression of bam, leading to aberrant germline differentiation.

391

392 **Discussion**

393 In this study, we identified Sakura, encoded by a previously uncharacterized gene *CG14545*, as an
394 essential factor for oogenesis and female fertility. We demonstrated that Sakura is specifically

395 expressed in germline cells in the ovary, including GSCs, is localized to the cytoplasm, and is
396 enriched in the developing oocytes. *sakura* homozygous null mutant flies are viable but completely
397 female-sterile and male-fertile. Loss of *sakura*, either through null mutation or germline RNAi
398 including in GSCs, results in rudimentary ovaries exhibiting germless and tumorous phenotypes.

399 The tumorous phenotype associated with the loss of *sakura* is characterized by an excess
400 of GSC-like cells, which feature round spectrosomes, as well as cyst cells with branched fusomes
401 (Fig 3C). The increased number of GSC-like cells in loss of *sakura* suggests dysregulation of GSC
402 self-renewal and differentiation. Meanwhile, the presence of excess cyst cells with branched
403 fusomes indicates abnormal differentiation and division of cysts. Differentiation of cystoblasts
404 typically involves four mitotic divisions with incomplete cytokinesis, leading to 16 cyst cells
405 interconnected by branched fusomes[7,46]. The degree of fusome branching serves as a marker for
406 the stages of cyst cell division, with increased branching from 2-cell to 16-cell cysts[47–49]. Notably,
407 fusomes begin to degenerate and disappear after 16-cell cysts as the germline cyst enters the
408 meiotic zone or region 2 of the germarium[50,51]. The persistence of cyst cells with branched fusomes
409 in *sakura*$^{null/null}$ suggests that *sakura* is crucial for the proper division and differentiation of cysts,
410 and we speculate that it is required for germline cysts to enter meiotic division.

411 Mosaic analysis of *sakura*^{null} indicates that *sakura* is intrinsically required for establishing
412 GSCs in the ovaries. A significantly reduced number of *sakura*^{null} marked GSCs were observed at
413 the adult stage when mutant clones were induced in PGC stages, suggesting that many *sakura*
414 mutant PGCs die before developing into GSCs. Furthermore, after inducing *sakura*^{null} clones in
415 adult ovaries, the number of marked *sakura*^{null} GSCs decreased at a higher rate than controls,
416 indicating a rapid loss of *sakura*^{null} GSCs (Fig 6A). Thus, *sakura* is also intrinsically necessary for
417 maintaining GSCs. Additionally, germaria containing *sakura*^{null} GSCs became increasingly

418 tumorous over time, with a growing number of *sakura*^{null} GSC-like cells (Fig 6B and 6C). This
419 suggests that *sakura*^{null} GSCs undergo uncontrolled division, becoming more tumorous over time,
420 which eventually triggers an intrinsic cell death mechanism, as evidenced by elevated levels of
421 cleaved Caspase-3 in *sakura*^{null} ovaries (Fig 3B).

422 Dpp/BMP signaling governs GSC self-renewal and cystoblast differentiation by repressing
423 *bam* in GSCs and de-repressing it in daughter cystoblasts (Fig S1). This process is mediated by the
424 transcription factor Mad, which, when phosphorylated (pMad), translocates into the nucleus to
425 repress *bam* transcription[7,46,52]. Our findings indicate that Bam expression is not limited to 8-cell
426 cysts but continues throughout the germarium in ovaries lacking *sakura* function (Fig 7A and 7B).
427 The persistent expression of Bam is likely due to low levels of pMad in GSCs (Fig 7C, and 7D).
428 Given the low pMad levels observed upon loss of *sakura*, we believe that the misregulation of
429 Bam expression occurs primarily at the transcriptional level, although it has also been reported
430 that Bam expression can be regulated post-transcriptionally[53].

431 Transposons are mobile genetic elements that, if not silenced, can generate DNA damage
432 and genomic instability[54]. piRNAs derived from transposons and other repeats can target and
433 silence transposon RNAs to preserve genome integrity in germ cells[31]. Loss of piRNAs leads to
434 transposon derepression, resulting in increased DNA damage, which subsequently triggers cell
435 death[55,56]. Genetic damage in germ cells can cause developmental defects and diseases that may
436 be inherited by the next generation. Thus, elimination of defective germ cells is crucial for
437 maintaining germline integrity of a species[57,58]. We found that loss of *sakura* results in reduced
438 piRNA levels and loss of piRNA-mediated transposon silencing in the germline (Fig 4). The
439 observed apoptosis, indicated by elevated cleaved Caspase-3 levels in *sakura* mutant ovaries (Fig
440 3B), suggest that desilencing of transposon due to reduced piRNA levels likely results in increased

441 DNA damage, triggering cell death. We speculate that the germless phenotype in *sakura* mutants
442 may partly arise from an apoptotic germline elimination program activated to maintain germline
443 integrity. Loss of *piwi*, a key component of the piRNA pathway, similarly causes GSC-like tumors,
444 as well as reduced *bam* expression and elevated pMad expression[29]. While downregulation of *bam*
445 and upregulation of pMad in *piwi* mutant is opposite to upregulation of *bam* and downregulation
446 of pMad in *sakura* mutant, defects in the piRNA pathway might be a shared underlying cause for
447 the dysregulation of *bam* and pMad levels in both cases, leading to tumorous phenotype.

448 In addition to its expression in GSCs and cysts in the germarium, Sakura is also expressed
449 in germline cells in later-stage egg chambers (Fig 1E-F) and is required at this stage for proper
450 oogenesis. When Sakura is depleted from region 2b of the germarium onward, while leaving GSCs
451 and early cyst cells intact, female flies lay significantly fewer eggs and have fewer stage 14 oocytes
452 (Fig 5). The failure to produce stage 14 oocytes likely results from the Orb mislocalization in
453 developing oocytes (Fig 5E). Orb is an RNA-binding protein crucial for egg chamber formation,
454 oocyte specification, and polarity establishment during oogenesis by regulating mRNA
455 localization and translation, such as that of *oskar*, which is vital for establishing oocyte anterior-
456 posterior polarity[34,59]. Interestingly, piRNA pathway mutants exhibit Orb mislocalization in
457 developing oocytes[60]. Therefore, reduced piRNA levels observed (Fig 4) may underlie the Orb
458 mislocalization in loss of *sakura* (Fig 5E).

459 Sakura does not possess any known protein domains, complicating investigations into its
460 molecular function. To infer its function, we identified interacting proteins through
461 immunoprecipitation followed by mass spectrometry. We identified Otu, a protein known to be
462 crucial for oogenesis, as a protein partner of Sakura. Mutations in *otu* gene lead to a range of
463 ovarian phenotypes, including germ cell loss, tumorous egg chambers filled with undifferentiated

464 germ cells, abnormalities in nurse cell chromosome structure, and defects in oocyte
465 determination[22,23]. We showed that germline depletion of Otu via RNAi phenocopies loss of
466 *sakura*. Similar to Sakura, loss of *otu* inhibits Dpp/BMP signaling, resulting in low pMad levels in
467 GSCs and Bam de-repression (Fig 12A-B). Additionally, loss of *otu* also results in the loss of
468 piRNA-mediated silencing, paralleling the effects of *sakura* loss. Furthermore, germline
469 knockdown of *otu* yielded a similar ratio of germless ovaries as seen in *sakura-RNAi,* and
470 simultaneous knockdown of both *otu* and *sakura* exacerbated the germless ovary phenotype (Fig
471 8). These observations raise the possibility that Sakura and Otu function together to regulate germ
472 cell maintenance in the ovaries and are involved in Dpp/BMP signaling to balance stem cell
473 renewal and differentiation.

474 Otu possesses deubiquitinase activity, catalyzed by its N-terminal Otu domain[21,61]. In germ
475 cells, Otu interacts with Bam, forming a deubiquitinase complex that deubiquitinates and thereby
476 stabilizes CycA, promoting GSC differentiation[21]. The predicted structure of Sakura and Otu
477 complex suggests that the Mid domain of Sakura directly contacts the Otu domain of Otu (Fig
478 10A). We found that Sakura lacks a deubiquitinase activity and it does not directly affect Otu's
479 deubiquitinase rate in our in vitro assays using Ub-Rhodamine 110 as a substrate (Fig S6). This
480 does not preclude the possibility that Sakura may still influence Otu's deubiquitinase activity,
481 potentially guiding Otu to its substrate and determining substrate specificity. Our in vitro assays
482 may not have detected such specificity changes. Otu is also an RNA-binding protein, and its
483 deubiquitinase activity can be enhanced by bound RNAs[7]. Future studies should explore whether
484 Sakura regulates Otu's RNA-binding or other RNA-related functions. Notably, while Otu is
485 expressed in various tissues, including testes and gut[42,61], Sakura is exclusively expressed in
486 ovaries, particularly in germline cells such as GSCs, Therefore, Sakura may enhance Otu's

487 functions specific to female germline cells. We believe that identifying Otu's deubiquitinase
488 substrates and its RNA partners, along with investigating Sakura's role in these processes, will
489 deepen our understanding of Sakura's and Otu's molecular functions in oogenesis. One speculative
490 hypothesis is that Sakura may regulate Otu's deubiquitinase activity concerning piRNA pathway
491 proteins crucial for proper piRNA production and function.

492 In summary, this study identifies and characterizes the previously unknown gene *sakura*,
493 which is specifically expressed in female germ cells and is essential for oogenesis and female
494 fertility. Together with its protein partner Otu, Sakura likely regulates germline cell fate,
495 maintenance, and differentiation

496

497 **Materials and Methods**

498 **Fly strains**

499 We generated the *sakura*^{null} strain by introducing indels within the Sakura coding region using the
500 CRISPR/Cas9 genome editing system, as we previously reported[26,62–65]. The transgenic *sakura-*
501 *EGFP, otu-EGFP,* and *otu(*Δ*-Tudor)-EGFP* strains were created following previously published
502 methods[65,66]. A fragment containing Sakura cDNA flanked by ~1 kbp upstream and ~1 kbp
503 downstream genomic sequences was cloned. Fragments containing Otu and Otu(Δ-Tudor) cDNAs,
504 flanked by ~2.5 kbp upstream and ~1 kbp downstream genomic sequences, were also cloned. The
505 EGFP gene was fused in-frame to the C-terminus of the Sakura and Otu coding sequences within
506 these fragments, which were then inserted into a pattB plasmid vector. The *sakura-EGFP* plasmid
507 was integrated into the 51C1 site within the fly genome using the BDSC:24482 fly strain and the

508 PhiC31 system, while the *otu-EGFP* and *otu(Δ-Tudor)-EGFP* plasmids were integrated into the
509 25C6 site of the genome using the attP40 fly strain and the PhiC31 system.

510 The *sakura RNAi* #1 (VDRC: v39727) and #2 (VDRC: v103660), *y-RNAi* (v106068), *TOsk-Gal4*
511 (v 314033), Burdock sensor [*UAS-Dcr2; NGT-Gal4; nosGal4-VP16, nos>NLS_GFP_lacZ_vas-*
512 *3'UTR_burdock-target*] (v 313217) strains were from Vienna *Drosophila* Resource Center. *w-RNAi*
513 (BDSC: 35573), *otu-RNAi* (BDSC: 34065), *bam-RNAi* (BDSC: 33631), *cycA-RNAi* (BDSC:
514 29313), *UAS-Dcr-2; NGT-Gal4* (BDSC: 25751), *FRT82B/TM6C, Sb* (BDSC: 86313) and otu^{14}
515 (BDSC: 6025) were obtained from the Bloomington Stock Center. The *bam-GFP* reporter (DGRC:
516 118177) and *vasa-EGFP* knocked-in fly (DGRC: 118616) were from Kyoto *Drosophila* Stock
517 Center.

518

519 **Fertility assay**

520 The female fertility assay was performed as previously described[64,65,67,68]. Briefly, five test virgin
521 females of each test genotype were mated with three wild-type (OregonR) males in a cage with a
522 6-cm grape juice agar plate supplemented with wet yeast paste. The agar plates were replaced
523 daily, and the number of eggs laid on the third plate (on day 3) was recorded. After incubation at
524 25°C for an additional day, the number of hatched eggs was counted. At least three cages per
525 genotype were tested.

526 For the male fertility assay, a single test male was mated with five wild-type (OregonR) virgin
527 females in each vial, following previously published methods[64,65,67]. After 3 days, the females were
528 transferred to a new vial (vial 1). Every two days, they were transferred to a new vial until a total
529 of four vials were obtained. After 2 days in the fourth vial, the females were removed, and the total

530 number of progenies emerging from these four vials was counted. At least five males per genotype
531 were tested.

532

533 **Sakura and Otu antibodies**

534 We expressed a recombinant full-length Sakura protein as an N-terminal 6xHis-tagged protein in
535 *E. coli* using a modified pET vector and purified it using Ni-sepharose (GE Healthcare) and
536 HiTrapQ HP (GE Healthcare) columns, as we previously performed for other proteins[64,65].
537 Recombinant Otu fragments (145-405aa and 406-853aa) were similarly expressed as N-terminally
538 6xHis-MBP-fusion proteins in *E. coli* and purified using Ni-sepharose. These purified proteins
539 were used as antigens to generate polyclonal anti-Sakura and anti-Otu sera in rabbits (Pocono
540 Rabbit Farm & Laboratory, Inc.). The rabbit polyclonal anti-Sakura antibodies were affinity
541 purified using His-MBP-Sakura recombinant protein and Affigel-15 (Bio-rad), following the
542 manufacturer's instructions. Rabbit anti-Otu sera were first pre-cleared with purified His-MBP
543 protein bound to Affigel-15, and the unbound fraction was affinity purified using purified His-
544 MBP-Otu fragments (145-405aa and 406-853aa) and Affigel-15.

545

546 **Germline clonal analysis**

547 We generated *sakura*^{null} mutant clones using FLP/FRT-mediated recombination[69]. To create
548 *sakura*^{null} GSC clones, 3-day-old female flies with the genotype *hs-flp*; *+; FRT82B, ubi-*
549 *GFP/FRT82B, sakura*^{null} were heat-shocked at 37°C for 1 hour, twice daily, with an 8-hour interval
550 between heat shocks. Female flies with the genotype *hs-flp*; +; *FRT82B, ubi-GFP/FRT82B* were
551 used as controls. Flies were dissected and stained 4, 7, and 14 days after clone induction. To induce

552 primordial germ cell (PGC) clones, early third-instar larvae were heat-shocked similarly, allowed
553 to develop, and dissected and analyzed at 3 to 4 days post-eclosion.

554

555 **Immunostaining**

556 Stereomicroscope images of dissected ovaries were taken using Leica M125 stereomicrocsope[64].
557 Ovaries from 2- to 5-day-old, yeast-fed females were hand-dissected in 1X PBS (137 mM NaCl,
558 2.7 mM KCl, 10 mM Na_2HPO_4, 1.8 mM KH_2PO_4, pH 7.4) at room temperature. The dissected
559 ovaries were fixed in a fixative buffer (4% formaldehyde, 15 mM PIPES (pH 7.0), 80 mM KCl,
560 20 mM NaCl2, 2 mM EDTA, and 0.5 mM EGTA), incubated for 30 minutes at room temperature
561 with gentle rocking. After fixation, the ovaries were rinsed three times with PBX (0.1% Triton X-
562 100 in 1X PBS) and then incubated in a blocking buffer (2% donkey serum in 3% BSA [w/v],
563 0.02% NAN3 [w/v] in PBX) for 1 hour at room temperature. Then, the ovaries were incubated
564 with primary antibodies diluted in the blocking buffer overnight at 4°C. The following day, the
565 ovaries were rinsed three times with PBX and incubated with Alexa Fluor-conjugated secondary
566 antibodies for 2 hours. The ovaries were rinsed three times with PBX and then mounted in
567 VECTASHIELD® PLUS antifade mounting medium with DAPI (H-2000, Vector lab). Confocal
568 images were acquired on a Zeiss LSM700 confocal microscope at the Johns Hopkins University
569 School of Medicine Microscope Facility.

570 The primary antibodies used for immunostaining were mouse anti-HTS (1B1) (DSHB,
571 AB_528070, 1/100), mouse anti-Bam (DSHB, AB_10570327, 1/20), mouse anti-CycA (DSHB,
572 AB_528188, 1/100), rat anti-Vasa (DSHB, AB_760351, 1/100), rabbit anti-pMad (Phospho-
573 SMAD1/5 (Ser463/465) mAb #9516, dilution: 1/200, Cell Signaling), and rabbit anti-cleaved

574 caspase-3 (Cleaved Caspase-3 (Asp175) #9661, dilution: 1/200, Cell Signaling). Secondary
575 antibodies used were Alexa Fluor 488 Donkey anti-Mouse Igg (ThermoFisher A21202, 1/100),
576 Alexa Fluor 594 Donkey anti-Rat Igg (ThermoFisher A21209, 1/100), Alexa Fluor 594 Donkey
577 anti-Mouse Igg (ThermoFisher A21203, 1/100), and Alexa Fluor 594 Donkey anti-Rabbit Igg
578 ThermoFisher A21207, 1/100).

579

580 **Western blot**

581 Lysates of hand-dissected ovaries and tissues were prepared by homogenizing in RIPA buffer (50
582 mM Tris-HCl [pH 7.4], 150 mM NaCl, 1% [v/v] IGEPAL CA-630, 0.1% [w/v] sodium dodecyl
583 sulfate (SDS), 0.5% [w/v] sodium deoxycholate, 1 mM ethylenediaminetetraacetic acid (EDTA),
584 5 mM dithiothreitol, and 0.5 mM phenylmethylsulfonyl fluoride (PMSF))[63–65,67]. The homogenates
585 were centrifuged at 21,000g at 4°C for 10 min, and the protein concentration of the supernatant
586 was determined using the BCA protein assay kit (Pierce) as needed. Fifteen μg of total protein was
587 loaded per lane for Western blot. The sources and dilutions of the primary antibodies were as
588 below. Rabbit anti-Sakura (1/10000, generated in this study), rabbit anti-Otu (1/10000, generated
589 in this study), rabbit anti-alpha-Tubulin [EP1332Y] (1/10000, Abcam, ab52866), mouse anti-
590 alpha-Tubulin [12G10] (1/10000, DSHB, AB_1157911), mouse anti-FLAG (1/10000, Sigma,
591 F1804), mouse anti-HA (1/10000, Sigma, H3663), and mouse anti-GFP [GF28R] (1/3000,
592 Invitrogen, 14-6674-82). IRDye 800CW goat anti-mouse IgG, IRDye 800CW goat anti-rabbit IgG,
593 IRDye 680RD goat anti-mouse, and IgG IRDye 680RD goat anti-rabbit were used as secondary
594 antibodies. The membranes were scanned using the Li-Cor Odyssey CLx Imaging System.

595

596 **Mass spectrometry**

597 Immunoprecipitation of Sakura-EGFP protein was performed using the GFP-Trap Magnetic
598 Agarose Kit (Proteintech, gtmak-20) on dissected ovaries from flies harboring *sakura-EGFP*
599 transgene, with *w1118* flies as controls. Ovaries were homogenized in 200 μL ice-cold lysis buffer
600 (10 mM Tris-HCl [pH 7.5], 150 mM NaCl, 0.5 mM EDTA, 0.05% [v/v] IGEPAL CA-630)
601 containing 1× protease inhibitor cocktail (100× protease inhibitor cocktail contains 120 mg/ml
602 1 mM 4-(2-aminoethyl) benzene sulfonyl fluoride hydrochloride (AEBSF), 1 mg/ml aprotinin,
603 7 mg/ml bestatin, 1.8 mg/ml E-64, and 2.4 mg/ml leupeptin)[70]. After homogenization, the tubes
604 were placed on ice for 30 minutes, and the homogenates were extensively pipetted every 10
605 minutes. The lysates were then centrifuged at 17,000x g for 10 minutes at 4°C. The supernatants
606 were transferred to pre-chilled tubes, and 300 μL dilution buffer (10 mM Tris/Cl pH 7.5, 150 mM
607 NaCl, 0.5 mM EDTA) supplemented with 1x protease inhibitor cocktail were added. The diluted
608 lysates were then added to the GFP-trap magnetic beads in 1.5 mL tubes and rotated for 1 hour at
609 4°C. After separating the beads with a magnetic tube rack, the beads were washed three times with
610 500 μL wash buffer (10 mM Tris/Cl pH 7.5, 150 mM NaCl, 0.05 % [v/v] IGEPAL CA-630).
611 Proteins were eluted with 40 μL acidic elution buffer (200 mM glycine pH 2.5) followed by
612 immediate neutralization with 5 uL neutralization buffer (1 M Tris pH 10.4).

613 As a quality control before mass spectrometry, ~5 μL of the samples were mixed with an
614 equal volume of 2× SDS-PAGE loading buffer (80 mM Tris-HCl [pH 6.8], 2% [w/v] SDS, 10%
615 [v/v] glycerol, 0.0006% [w/v] bromophenol blue, 2% [v/v] 2-mercaptoethanol), heated at 95 °C
616 for 3 min, and run on 4–20% Mini-PROTEAN® TGX™ Precast Protein Gels (Biorad, #4561094).
617 Silver staining was then performed by using Pierce™ Silver Stain Kit (ThermoFisher, 24612) to
618 assess the quality of the immunoprecipitated protein samples. Mass spectrometry was conducted

619 at the Mass Spectrometry Core at the Department of Biological Chemistry, Johns Hopkins School
620 of Medicine, as previously described[65]

621

622 **Co-immunoprecipitation**

623 For co-immunoprecipitation of endogenous Sakura protein, wild-type ovaries (*w1118*) were
624 homogenized in RIPA buffer, centrifuged at 21,000g at 4°C for 10 min, and the clear supernatant
625 protein lysates were used for immunoprecipitation. Four μg of rabbit anti-Sakura and normal rabbit
626 IgG (Cell Signaling, #2729) were incubated with 50 μL of Dynabeads Protein G (ThermoFisher,
627 10004D) for 20 min at room temperature. The beads were washed once with PBST (1x PBS with
628 0.1% Tween-20). The ovary lysate supernatant was then incubated with the washed beads at room
629 temperature for 30 min, followed by three washes with PBST. The proteins were eluted with 2x
630 SDS-PAGE loading buffer (80 mM Tris-HCl [pH 6.8], 2% [w/v] SDS, 10% [v/v] glycerol,
631 0.0006% [w/v] bromophenol blue, 2% [v/v] 2-mercaptoethanol) and heated at 70°C for 10 min.
632 After bead separation using a magnetic tube rack, the eluted proteins in 2x SDS-PAGE loading
633 buffer were heated again at 95°C for 3 min.

634 Transient protein expression in S2 cells was performed using the pAc5.1/V5-HisB plasmid
635 vector (Invitrogen). A total of 1 μg plasmids were transfected using the Effectene transfection
636 reagent (Qiagen, 301425). Three days after transfection, cells were harvested and lysed with ice-
637 cold lysis buffer supplemented with 1× protease inhibitor cocktail. The cell lysates were then
638 centrifuged at 17,000x g for 10 min at 4°C, and the clear supernatants were collected for
639 immunoprecipitation. For anti-HA immunoprecipitation, supernatants were incubated with 25 μL
640 (0.25 mg) of Pierce™ Anti-HA Magnetic Beads (ThermoFisher, 88837) at room temperature for

641 30 min. The beads were then washed three times with TBST (1x TBS [0.05 M Tris/HCl and 0.15
642 M NaCl, pH 7.6] with 0.05% Tween-20). For anti-FLAG immunoprecipitation, 2 μg of mouse anti-
643 FLAG (1/10000, Sigma, F1804) was incubated with 50 μL of Dynabeads Protein G
644 (ThermoFisher, 10004D) for 10 min at room temperature. The beads were washed once with
645 PBST. The S2 cell lysate supernatant was incubated with the washed beads at room temperature
646 for 15 min. The beads were washed three times with PBST. In both anti-HA and anti-FLAG
647 immunoprecipitations, proteins were eluted with 2× SDS-PAGE loading buffer. For anti-HA, the
648 beads in 2x SDS-PAGE loading buffer were heated at 95°C for 7 min. For anti-FLAG, the beads
649 were heated at 70°C for 10 min, then were separated using a magnetic tube rack. The eluted
650 proteins in 2x SDS-PAGE loading buffer were heated again at 95°C for 3 min.

651

652 **Small RNA and mRNA sequencing**

653 Poly-A+ mRNA purification was performed as previously described[71]. Small RNA libraries and
654 poly-A+ mRNA libraries were prepared, sequenced on Hiseq2500 (Illumina), and analyzed, as
655 previously reported[72,73]. SRA accession number for these datasets is PRJNA1156618.

656

657 **In vitro deubiquitination assay**

658 C-terminally 6xHis-tagged recombinant Sakura protein was expressed in *E. coli* using a modified
659 pET vector and was purified using Ni-sepharose. N-terminally 3xHA-HRV3Csite-3xFLAG-
660 tagged Otu protein and a negative control, N-terminally 3xHA-HRV3Csite-3xFLAG-tagged
661 firefly luciferase protein, were expressed in S2 cells using pAc5.1/V5-HisB vector. The proteins
662 were immunoprecipitated using Pierce™ Anti-HA Magnetic Beads (ThermoFisher, 88837) as

663 described previously, with a more stringent washing step to effectively remove interacting proteins.
664 The beads were washed six times with a high salt wash buffer (TBST with 800 mM NaCl). The
665 proteins were eluted by cleaving off 3xHA tag with 25 nM GST-HRV3C protease in a cleavage
666 buffer (25mM Tris-HCl pH 7.4, 150 mM NaCl, 5% glycerol, 2mM EDTA), incubated at 4°C with
667 rotation for 6 hours. An equal volume of 100% glycerol was added to the eluted protein.

668 Purified proteins, including Otu, luciferase, and Sakura, were mixed with Ub-Rhodamine
669 110 (Ubiquitin-Proteasome Biotechnologies, M3020) in a total volume of 30 μL in reaction buffer
670 (20 mM Tris-HCl, pH 7.5, 200 mM NaCl, 5 mM $MgCl_2$, 2 mM DTT). The mixture was added to
671 a black 384-well low-volume plate. Fluorescence measurements were taken using SpectraMax i3x
672 Multi-Mode Microplate Reader at 37°C, with excitation and emission wavelengths set at 485/20
673 and 530/20 nm respectively. The fluorescence intensity for each condition was averaged from
674 triplicates and plotted as a function of time.

675

676 **Acknowledgments**

677 We thank Bloomington Drosophila Stock Center, Vienna Drosophila Resource Center, and Kyoto
678 Drosophila Stock Center for fly strain stocks. We thank the Johns Hopkins University School of
679 Medicine Microscope Facility for use of the Zeiss LSM700, supported by NIH grant
680 S10OD016374 awarded to Dr. Scot C. Kuo. We thank Ms. Lauren DeVine and Dr. Bob Cole at the
681 Johns Hopkins University School of Medicine Mass Spectrometry and Proteomics Core Facility
682 for the mass-spec analysis. This work was supported by the grants from the National Institutes of
683 Health [R35GM145352] and Johns Hopkins University Catalyst Award to RF.

684

685 **Author Contributions**

686 Methodology and Investigation, A.A., L.Z., and R.F.; Conceptualization and Writing, A.A. and
687 R.F.; Funding Acquisition and Supervision, R.F.

688

689 **Competing interests**

690 The authors have no conflicts of interest to declare.

691

692 **Figure Legends**

693 **Fig 1. Sakura expression pattern and mutant allele**

694 (A) *Drosophila* Sakura protein (Sakura/CG14545) and its null mutant allele generated in this study.
695 (B) *sakura* mRNA expression pattern. Data obtained from
696 http://flybase.org/reports/FBgn0040602.htm. (C) Western blot of dissected fly tissues. (D) Western
697 blot of ovary lysates. (E) Confocal images of the germarium from the *sakura-EGFP* transgenic fly.
698 Sakura-EGFP (green), Hts (red), and DAPI (blue). Scale bar: 10 μm. (F) Confocal images of the
699 egg chambers from the *sakura-EGFP* transgenic fly. Sakura-EGFP (green), Vasa (red), and DAPI
700 (blue). Sakura-EGFP is expressed in nurse cells and enriched in the developing oocyte (yellow
701 arrow). Scale bar: 20 μm.

702

703 **Fig 2. *sakura* mutant flies are female-sterile and have rudimentary ovaries.**

704 (A-B) Female fertility assays. (A) The number of eggs laid by test females crossed with OregonR
705 wild-type males and (B) hatching rates of the eggs. Mean ± SD (n = 3). P-value < 0.05 (Student's
706 t-test, unpaired, two-tailed) is indicated by *. (C) Stereomicroscope images of dissected whole
707 ovaries. Scale bar: 1 mm.

708

709 **Fig 3. *sakura*^{null} ovaries are germless and tumorous**

710 (A) Confocal images of the ovaries from control (*sakura*$^{null/+}$) and *sakura*$^{null/null}$ harboring *vasa-*
711 *EGFP*. Vasa-EGFP (green) and DAPI (blue). Yellow stars label the anterior tip of the ovaries. Scale
712 bar: 100 μm. (B) Confocal images of *sakura*$^{null/null}$ ovaries stained with anti-cleaved Caspase-3
713 antibody. Cleaved caspase-3 (green) and DAPI (blue). Control ovary is *sakura*$^{null/+}$. Yellow stars
714 label the anterior tip of the ovaries. Scale bars: 20 μm for control and 100 μm for *sakura*$^{null/null}$. (C)
715 Confocal images of control (*sakura*$^{null/+}$) and *sakura*$^{null/null}$ ovaries stained with anti-Hts antibody
716 to label spectrosomes and fusomes. Hts (red) and DAPI (blue). Yellow star labels the anterior tip
717 in the control ovary. Red and green stars label the anterior tip of *sakura*$^{null/null}$ tumorous and
718 germless ovarioles, respectively. Scale bars: 20 μm for control and 50 μm for *sakura*$^{null/null}$. (D)
719 Ratio (%) of normal, germless, and tumorous ovaries of indicated genotypes (n=33, 25, 74, 29
720 respectively). (E) Quantification of GSC-like cell number in germaria of indicated genotypes (n =
721 33, 30, 35, and 31 respectively).

722

723 **Fig 4. Loss of *sakura* results in lower piRNA levels and loss of piRNA-mediated transposon**
724 **silencing**

725 (A) Scatter plots of normalized number of transposon piRNA reads from small RNA-seq of
726 indicated genotypes compared with *sakura*$^{+/+}$. Means of three biological replicates are plotted.
727 Downregulated (fold-change < 0.5) and upregulated (fold-change > 2) transposon piRNAs are
728 shown in cyan and magenta, respectively. (B) Volcano plots of transposon RNAs from RNA-seq
729 of indicated genotypes compared with *sakura*$^{+/+}$. Three biological replicates per genotype were
730 analyzed. Downregulated (adjusted p-value < 0.001 and $\log_2$(fold-change) < -2) and upregulated
731 (adjusted p-value < 0.001 and $\log_2$(fold-change) > 2) transposons are shown in cyan and magenta,
732 respectively. (C) Normalized number of reads for *Burdock* piRNAs from small RNA-seq.
733 Mean ± SD (n = 3.) P-value < 0.05 (Student's t-test, unpaired, two-tailed) is indicated by *. (D) The
734 *Burdock* sensor harbors a *nanos* promoter, a nuclear localization signal (NLS) appended to GFP
735 and β-gal coding sequences, and a target sequence for *Burdock* piRNAs in the 3'UTR. Confocal
736 images of ovaries from control (y^{RNAi}) and *sakura*^{RNAi} flies harboring the Burdock sensor, where
737 RNAi knockdown was specifically driven in the female germline with *UAS-Dcr2* and *NGT-Gal4*.
738 GFP (green), β-gal (red), and DAPI (blue). Scale bar: 50 μm.

739

740 **Fig 5. *sakura* is important for oogenesis in later-stage egg chambers**

741 (A) Stereomicroscope images of dissected whole ovaries. Scale bar: 500 μm. (B) Western blot of
742 dissected ovary lysates. *sakura*$^{RNAi\ \#1}$ and *sakura*$^{RNAi\ \#2}$ are two independent RNAi lines. (C)
743 Number of eggs laid by *sakura* RNAi knockdown driven by *UAS-Dcr2* and *TOsk-Gal4*.
744 Mean ± SD (n = 5). P-value < 0.05 (Student's t-test, unpaired, two-tailed) is indicated by *. (D)
745 Number of stage 14 oocytes produced by *sakura* RNAi knockdown flies driven by *UAS-Dcr2* and
746 *TOsk-Gal4*. P-value < 0.05 (Student's t-test, unpaired, two-tailed) is indicated by *. (E) Confocal
747 images of the ovaries from *sakura* RNAi knockdown flies driven by *UAS-Dcr2* and *TOsk-Gal4*,

748 stained with anti-Orb and anti-Vasa antibodies. Orb (green), Vasa (red), and DAPI (blue). Yellow
749 arrows label the localization and enrichment of Orb in the developing oocytes. Scale bar: 100 μm.
750 In A-E, *y-RNAi* was used as a control.

751

752 **Fig 6. Germline clonal analysis of *sakura*^{null}**

753 (A) Percentage of germaria with marked GSC clones indicated by the absence of GFP at 4, 7, and
754 14 days after clone induction at the adult stage. Arrows indicate the percent decrease of marked
755 GSC clones compared to day 4. The genotype, actual percentage, and total number of germaria
756 examined are shown in the adjacent table. (B) Confocal images of germ cell clones. *sakura*^{null} and
757 control clones were marked by the absence of GFP. GFP (green), Hts (red), and DAPI (blue). Scale
758 bar: 20 μm. (C) Number of marked (GFP-negative) GSC-like cells in germaria with marked GSCs
759 of the indicated genotypes at 4, 7, and 14 days after clone induction. GSC-like cells containing
760 round spectrosome were identified through immunostaining with anti-Hts antibody. P-value < 0.05
761 (Student's t-test, unpaired, two-tailed) is indicated by *.

762

763 **Fig 7. Loss of *sakura* inhibits Dpp/BMP signaling**

764 (A) Confocal images of ovaries from control (y^{RNAi}) and *sakura*^{RNAi} flies harboring the *bam-GFP*
765 reporter, where RNAi knockdown was specifically driven in the female germline with *UAS-Dcr2*
766 and *NGT-Gal4*. Bam-GFP (green), Hts (red), and DAPI (blue). Scale bar: 20 μm. (B, C) Confocal
767 images of germaria with germline clones of *sakura*^{null} stained with (B) anti-Bam antibody and (C)
768 anti-pMad antibody. GFP (green), Bam or pMad (red), and DAPI (blue). Scale bar: 10 μm. (D)
769 Mean pMad intensity in the germline clones of the indicated genotypes. Mean ± SD ($n = 7$). P-

770 value < 0.05 (Student's t-test, unpaired, two-tailed) is indicated by * (E) Confocal images of
771 germaria with germline clones of *sakura*^{null} stained with anti-CycA antibody. GFP (green), CycA
772 (red), and DAPI (blue). Scale bar: 10 μm. (F) Mean CycA intensity in the germline clones of the
773 indicated genotypes. Mean ± SD (n = 5 and 10 for *FRT82B* and *FRT82B, sakura*^{null} respectively).
774 P-value < 0.05 (Student's t-test, unpaired, two-tailed) is indicated by *. In B, C, and E, clones were
775 marked with the absence of GFP.

776

777 **Fig 8. The ratio of ovary germless phenotype from double RNAi knockdown of *sakura* with**
778 ***bam*, *cycA*, or *otu***

779 Mean ratio (%) of ovaries with the germless phenotype observed in double RNAi knockdown of
780 *sakura* with *bam, cycA,* or *otu. UAS-Dcr2* and *NGT-Gal4* was used to drive RNAi knockdown in
781 the germline. n is the total number of ovaries examined for the indicated genotypes. Three
782 independent crosses (biological replicates) were set up to generate the flies with genotypes of
783 interest, and the ratio of ovaries with the germless phenotype in each replicate was calculated.
784 Mean ± SD (three biological replicates). P-value < 0.05 (Student's t-test, unpaired, two-tailed) is
785 indicated by *.

786

787 **Fig 9. Sakura interacts with Otu.**

788 (A) Co-immunoprecipitation using anti-GFP magnetic beads followed by Western blotting. Ovary
789 lysates expressing Sakura-EGFP and those from w^{1118} negative control were tested. (B) Co-
790 immunoprecipitation using beads bound with rabbit anti-Sakura followed by Western blotting.
791 Ovary lysates from w^{1118} flies were used. Rabbit IgG was used as control IP. (C) Co-

792 immunoprecipitation using beads bound with anti-FLAG antibody followed by Western blotting.
793 S2 cell lysates expressing 3xFLAG-Otu and Sakura-mCherry-3xHA or mCherry-3xHA (negative
794 control) were used.

795

796 **Fig 10. N-terminal regions of Sakura and Otu are important for interaction.**

797 (A) Predicted structure of the Sakura and Otu protein complex made by AlphaFold. Full-length
798 Sakura and N-terminal Otu fragment (N1. 1-405aa) were used for prediction. (B) Full-length Otu
799 and Otu fragments tested in co-immunoprecipitation assays. (C) Full-length Sakura and Sakura
800 fragments tested in co-immunoprecipitation assays (N: N-terminal, M: middle, C: C-terminal). (D,
801 E, F) Co-immunoprecipitation using anti-HA magnetic beads followed by Western blotting. S2
802 cell lysates expressing HA-tagged mCherry were used as negative controls.

803

804 **Fig 11. Loss of *otu* phenocopies loss of *sakura***

805 (A) Confocal images of ovaries from *otu-EGFP* and *otu(ΔTudor)-EGFP* transgenic flies. Otu-
806 EGFP and Otu(ΔTudor)-EGFP (green), DAPI (blue). Yellow arrows show the enrichment of Otu-
807 EGFP and Otu(ΔTudor)-EGFP in developing oocytes. Scale bar: 20 μm. (B) Stereomicroscope
808 images of dissected whole ovaries from w^{RNAi} (control) and otu^{RNAi} flies where RNAi knockdown
809 was driven in the female germline with *nos-Gal4-VP16* or *TOsk-Gal4*. Scale bar: 500 μm. (C)
810 Number of eggs laid by *TOsk-Gal4* > w^{RNAi} and *TOsk-Gal4* > otu^{RNAi} flies. Mean ± SD (n = 5). P-
811 value < 0.05 (Student's t-test, unpaired, two-tailed) are indicated by *. (D) Violin plots of the
812 number of stage 14 oocytes produced in *TOsk-Gal4* > w^{RNAi} and *TOsk-Gal4* > otu^{RNAi} flies. n = 30.
813 P-value < 0.05 (Student's t-test, unpaired, two-tailed) is indicated by *. (E) Confocal images of the

814 ovaries from w^{RNAi} (control) and otu^{RNAi} flies harboring the Burdock sensor where RNAi
815 knockdown was driven in the female germline with *UAS-Dcr2* and *NGT-Gal4*. GFP (green), β-gal
816 (red), and DAPI (blue). Scale bar: 50 μm. (F) Confocal images of the ovaries from *nos-Gal4-VP16*
817 > w^{RNAi} and *nos-Gal4-VP16* > otu^{RNAi} flies stained with anti-cleaved Caspase 3 antibody. Cleaved
818 Caspase-3 (green) and DAPI (blue). Scale bar: 20 μm

819

820 **Fig 12. Loss of *otu* results in low levels of pMad and derepression of *bam* in the germaria**

821 (A) Confocal images of the ovaries from control (w^{RNAi}) and otu^{RNAi} flies harboring the *bam-GFP*
822 reporter, where RNAi knockdown was driven in the female germline with *nos-Gal4-VP16*. Bam-
823 GFP (green), Hts (red), and DAPI (blue). Scale bar: 20 μm. (B) Confocal images of germaria from
824 control ($otu^{14/+}$) and $otu^{14/14}$ mutant flies stained with anti-pMad (green) and anti-Hts (red)
825 antibodies. Scale bar: 10 μm.

826

827 **Fig S1. Schematic illustration of Drosophila ovary and germarium**

828 (A) Drosophila female has a pair of ovaries, each composed of 12-16 ovarioles. The germarium is
829 located at the anterior tip of the ovarioles and consists of germ cells and somatic cells. Germline
830 stem cells (GSCs), cystoblasts, cysts, and more differentiate oocytes are germ cells, while terminal
831 filament cells, cap cells, escort cells, and follicle cells are somatic cells. GSCs and cystoblasts have
832 round-shaped and unbranched spectrosomes, while cysts have branched fusomes. (B) Cap cells
833 secrete diffusible Decapentaplegic (Dpp), which is received by its receptor, a heterodimer of Thick
834 vein (Tkv) and Punt (Put), in GSCs. The activated Dpp signaling eventually phosphorylates
835 Mother-against-dpp (Mad). The phosphorylated Mad (pMad) represses the transcription of *bag-*

836 *of-marbles* (*bam*). The repression of *bam* in GSCs is crucial for maintaining their stemness.
837 Cystoblasts do not receive Dpp, and Bam expression is crucial for promoting cystoblast
838 differentiation from GSCs.

839

840 **Fig S2. Male fertility assay.**

841 The numbers of the progeny flies obtained from crosses between test males and wild-type
842 (OregonR) virgin females are shown. Mean ± SD (n = 5).

843

844 **Fig S3. *sakura*^{null} ovaries are tumorous**

845 Violin plots of GSC-like cell numbers in germaria of indicated genotypes. Mean ± SD and the
846 biological replicate number n are also shown. P-value < 0.05 (Student's t-test, unpaired, two-tailed)
847 is indicated by *

848

849 **Fig S4. *sakura*^{null} clone germline cells intrinsically cause tumorous phenotype**

850 Violin plots of GSC-like cell number in germaria of indicated genotypes. Mean ± SD, and the
851 biological replicated number n are also shown. P-value < 0.05 (Student's t-test, unpaired, two-
852 tailed) are indicated by *

853

854 **Fig S5. Co-immunoprecipitations assay to test interaction between N-terminal fragments of**
855 **Sakura and Otu in S2 cells**

856 Co-immnuprocepitation assay using beads bound with anti-FLAG antibody followed by Western
857 blotting. S2 cell lysates expressing mCherry-3xHA were used as controls. This is the reciprocal
858 co-immunoprecipitation of Fig 10F.

859

860 **Fig S6. In vitro deubiquitination assay.**

861 The mean fluorescence intensity of three replicates was plotted. Error bars (+/-) are standard
862 deviations. Firefly Luciferase was used as a negative control.

863

Identified protein name	Gene ID	Unique peptide counts					
		Sakura-EGFP samples			w1118 samples (negative control)		
		Replicate 1	Replicate 2	Replicate 3	Replicate 1	Replicate 2	Replicate 3
Ovarian tumor	CG12743	44	38	18	0	0	0
Uncharacterized protein Dmel_CG4679	CG4679	17	8	2	0	0	0
Uncharacterized protein Dmel_CG14997	CG14997	17	7	2	0	0	0
Mitochondrial ribosomal protein S22	CG12261	14	6	1	0	0	0
Tudor	CG9450	15	1	1	0	0	0
Mitochondrial ribosomal protein S5	CG40049	10	4	1	0	0	0
HECT and RLD domain containing protein 2	CG11734	4	9	1	0	0	0
Mitochondrial ribosomal protein S10	CG4247	5	3	1	0	0	0
Mitochondrial ribosomal protein S31	CG5904	3	1	1	0	0	0

Uncharacterized protein Dmel_CG1316	CG1316	2	1	1	0	0	0

Table 1. **Number of unique peptide counts detected by mass-spec**.

Proteins with peptide signals present in all three biological replicates of the Sakura-EGFP samples without any signals in any of the three biological replicates of the negative control are shown.

870

871 **References**

872 1. Lin, H. & Spradling, A. C. Germline Stem Cell Division and Egg Chamber Development in Transplanted
873 *Drosophila* Germaria. *Dev. Biol.* **159**, 140–152 (1993).
874 2. de Cuevas, M. & Matunis, E. L. The stem cell niche: lessons from the Drosophila testis. *Development*
875 **138**, 2861–2869 (2011).
876 3. Losick, V. P., Morris, L. X., Fox, D. T. & Spradling, A. Drosophila Stem Cell Niches: A Decade of
877 Discovery Suggests a Unified View of Stem Cell Regulation. *Dev. Cell* **21**, 159–171 (2011).
878 4. Schüpbach, T., Wieschaus, E. & Nöthiger, R. A study of the female germ line in mosaics of Drosophila.
879 *Wilhelm Rouxs Arch. Dev. Biol.* **184**, 41–56 (1978).
880 5. Spradling, A. C. Germline cysts: Communes that work. *Cell* **72**, 649–651 (1993).
881 6. Lin, H., Yue, L. & Spradling, A. C. The Drosophila fusome, a germline-specific organelle, contains
882 membrane skeletal proteins and functions in cyst formation. *Development* **120**, 947–956 (1994).
883 7. Kirilly, D. & Xie, T. The Drosophila ovary: an active stem cell community. *Cell Res.* **17**, 15–25 (2007).
884 8. Lin, H. The Tao of stem cells in the germline. *Annu. Rev. Genet.* **31**, 455–491 (1997).
885 9. Cox, D. N. *et al.* A novel class of evolutionarily conserved genes defined by piwi are essential for stem
886 cell self-renewal. *Genes Dev.* **12**, 3715–3727 (1998).
887 10. Gateff, E. *et al.* Drosophila differentiation genes instrumental in tumor suppression. *Int. J. Dev. Biol.*
888 **40**, 149–156 (1996).
889 11. Ohlstein, B., Lavoie, C. A., Vef, O., Gateff, E. & McKearin, D. M. The Drosophila cystoblast
890 differentiation factor, benign gonial cell neoplasm, is related to DExH-box proteins and interacts
891 genetically with bag-of-marbles. *Genetics* **155**, 1809–1819 (2000).

892 12. Song, X., Zhu, C.-H., Doan, C. & Xie, T. Germline Stem Cells Anchored by Adherens Junctions in the
893 Drosophila Ovary Niches. *Science* **296**, 1855–1857 (2002).
894 13. Gilboa, L., Forbes, A., Tazuke, S. I., Fuller, M. T. & Lehmann, R. Germ line stem cell differentiation in
895 Drosophila requires gap junctions and proceeds via an intermediate state. *Development* **130**, 6625–
896 6634 (2003).
897 14. Xie, T. & Spradling, A. C. decapentaplegic Is Essential for the Maintenance and Division of Germline
898 Stem Cells in the Drosophila Ovary. *Cell* **94**, 251–260 (1998).
899 15. Casanueva, M. O. & Ferguson, E. L. Germline stem cell number in the Drosophila ovary is regulated
900 by redundant mechanisms that control Dpp signaling. *Development* **131**, 1881–1890 (2004).
901 16. Kai, T. & Spradling, A. An empty Drosophila stem cell niche reactivates the proliferation of ectopic
902 cells. *Proc. Natl. Acad. Sci.* **100**, 4633–4638 (2003).
903 17. Song, X. *et al.* Bmp signals from niche cells directly repress transcription of a differentiation-
904 promoting gene, bag of marbles, in germline stem cells in the Drosophila ovary. *Development* **131**,
905 1353–1364 (2004).
906 18. McKearin, D. M. & Spradling, A. C. bag-of-marbles: a Drosophila gene required to initiate both male
907 and female gametogenesis. *Genes Dev.* **4**, 2242–2251 (1990).
908 19. Ohlstein, B. & McKearin, D. Ectopic expression of the Drosophila Bam protein eliminates oogenic
909 germline stem cells. *Development* **124**, 3651–3662 (1997).
910 20. McKearin, D. & Ohlstein, B. A role for the Drosophila Bag-of-marbles protein in the differentiation of
911 cystoblasts from germline stem cells. *Development* **121**, 2937–2947 (1995).
912 21. Ji, S. *et al.* Bam-dependent deubiquitinase complex can disrupt germ-line stem cell maintenance by
913 targeting cyclin A. *Proc. Natl. Acad. Sci.* **114**, 6316–6321 (2017).
914 22. King, R. C. & Riley, S. F. Ovarian pathologies generated by various alleles of the otu locus in
915 Drosophila melanogaster. *Dev. Genet.* **3**, 69–89 (1982).

916 23. Glenn, L. E. & Searles, L. L. Distinct domains mediate the early and late functions of the *Drosophila*
917 *ovarian tumor* proteins. *Mech. Dev.* **102**, 181–191 (2001).
918 24. Storto, P. D. & King, R. C. Multiplicity of functions for the otu gene products during Drosophila
919 oogenesis. *Dev. Genet.* **9**, 91–120 (1988).
920 25. Rodesch, C., Pettus, J. & Nagoshi, R. N. The Drosophila*ovarian tumor*Gene Is Required for the
921 Organization of Actin Filaments during Multiple Stages in Oogenesis. *Dev. Biol.* **190**, 153–164 (1997).
922 26. Kondo, S. & Ueda, R. Highly Improved Gene Targeting by Germline-Specific Cas9 Expression in
923 Drosophila. *Genetics* **195**, 715–721 (2013).
924 27. Yang, F. *et al.* Ovaries absent links dLsd1 to HP1a for local H3K4 demethylation required for
925 heterochromatic gene silencing. *eLife* **8**, e40806 (2019).
926 28. Eliazer, S., Shalaby, N. A. & Buszczak, M. Loss of lysine-specific demethylase 1 nonautonomously
927 causes stem cell tumors in the Drosophila ovary. *Proc. Natl. Acad. Sci.* **108**, 7064–7069 (2011).
928 29. Jin, Z., Flynt, A. S. & Lai, E. C. Drosophila piwi mutants exhibit germline stem cell tumors that are
929 sustained by elevated Dpp signaling. *Curr. Biol. CB* **23**, 1442–1448 (2013).
930 30. Handler, D. *et al.* The Genetic Makeup of the Drosophila piRNA Pathway. *Mol. Cell* **50**, 762–777
931 (2013).
932 31. Siomi, M. C., Sato, K., Pezic, D. & Aravin, A. A. PIWI-interacting small RNAs: the vanguard of genome
933 defence. *Nat. Rev. Mol. Cell Biol.* **12**, 246–258 (2011).
934 32. Dönertas, D., Sienski, G. & Brennecke, J. Drosophila Gtsf1 is an essential component of the Piwi-
935 mediated transcriptional silencing complex. *Genes Dev.* **27**, 1693–1705 (2013).
936 33. ElMaghraby, M. F., Tirian, L., Senti, K.-A., Meixner, K. & Brennecke, J. A genetic toolkit for studying
937 transposon control in the Drosophila melanogaster ovary. *Genetics* **220**, iyab179 (2021).
938 34. Barr, J., Gilmutdinov, R., Wang, L., Shidlovskii, Y. & Schedl, P. The Drosophila CPEB Protein Orb
939 Specifies Oocyte Fate by a 3'UTR-Dependent Autoregulatory Loop. *Genetics* **213**, 1431–1446 (2019).

940 35. Xu, T. & Rubin, G. M. Analysis of genetic mosaics in developing and adult Drosophila tissues.
941 *Development* **117**, 1223–1237 (1993).
942 36. Yang, L. *et al.* Argonaute 1 regulates the fate of germline stem cells in Drosophila. *Development* **134**,
943 4265–4272 (2007).
944 37. Hayashi, Y., Yoshinari, Y., Kobayashi, S. & Niwa, R. The regulation of *Drosophila* ovarian stem cell
945 niches by signaling crosstalk. *Curr. Opin. Insect Sci.* **37**, 23–29 (2020).
946 38. Chen, D. & McKearin, D. M. A discrete transcriptional silencer in the bam gene determines
947 asymmetric division of the Drosophila germline stem cell. *Development* **130**, 1159–1170 (2003).
948 39. Chen, D. *et al.* Effete-mediated degradation of Cyclin A is essential for the maintenance of germline
949 stem cells in Drosophila. *Development* **136**, 4133–4142 (2009).
950 40. Chen, D. & McKearin, D. Dpp Signaling Silences bam Transcription Directly to Establish Asymmetric
951 Divisions of Germline Stem Cells. *Curr. Biol.* **13**, 1786–1791 (2003).
952 41. Xia, L. *et al.* The Fused/Smurf Complex Controls the Fate of Drosophila Germline Stem Cells by
953 Generating a Gradient BMP Response. *Cell* **143**, 978–990 (2010).
954 42. Steinhauer, W. R. & Kalfayan, L. J. A specific ovarian tumor protein isoform is required for efficient
955 differentiation of germ cells in Drosophila oogenesis. *Genes Dev.* **6**, 233–243 (1992).
956 43. Buskirk, C. V. & Schüpbach, T. half pint Regulates Alternative Splice Site Selection in Drosophila. *Dev.*
957 *Cell* **2**, 343–353 (2002).
958 44. Sass, G. L., Comer, A. R. & Searles, L. L. The Ovarian Tumor Protein Isoforms of *Drosophila*
959 *melanogaster* Exhibit Differences in Function, Expression, and Localization. *Dev. Biol.* **167**, 201–212
960 (1995).
961 45. Jumper, J. *et al.* Highly accurate protein structure prediction with AlphaFold. *Nature* **596**, 583–589
962 (2021).

963 46. Hinnant, T. D., Merkle, J. A. & Ables, E. T. Coordinating Proliferation, Polarity, and Cell Fate in the
964 Drosophila Female Germline. *Front. Cell Dev. Biol.* **8**, (2020).
965 47. Christophorou, N., Rubin, T. & Huynh, J.-R. Synaptonemal Complex Components Promote
966 Centromere Pairing in Pre-meiotic Germ Cells. *PLoS Genet.* **9**, e1004012 (2013).
967 48. Hinnant, T. D., Alvarez, A. A. & Ables, E. T. Temporal remodeling of the cell cycle accompanies
968 differentiation in the *Drosophila* germline. *Dev. Biol.* **429**, 118–131 (2017).
969 49. Mathieu, J., Michel-Hissier, P., Boucherit, V. & Huynh, J.-R. The deubiquitinase USP8 targets ESCRT-III
970 to promote incomplete cell division. *Science* (2022) doi:10.1126/science.abg2653.
971 50. Cuevas, M. de & Spradling, A. C. Morphogenesis of the Drosophila fusome and its implications for
972 oocyte specification. *Development* **125**, 2781–2789 (1998).
973 51. Snapp, E. L., Iida, T., Frescas, D., Lippincott-Schwartz, J. & Lilly, M. A. The Fusome Mediates
974 Intercellular Endoplasmic Reticulum Connectivity in Drosophila Ovarian Cysts. *Mol. Biol. Cell* **15**,
975 4512–4521 (2004).
976 52. Kahney, E. W., Snedeker, J. C. & Chen, X. Regulation of *Drosophila* germline stem cells. *Curr. Opin. Cell*
977 *Biol.* **60**, 27–35 (2019).
978 53. Pek, J. W., Lim, A. K. & Kai, T. Drosophila Maelstrom Ensures Proper Germline Stem Cell Lineage
979 Differentiation by Repressing microRNA-7. *Dev. Cell* **17**, 417–424 (2009).
980 54. Levin, H. L. & Moran, J. V. Dynamic interactions between transposable elements and their hosts. *Nat.*
981 *Rev. Genet.* **12**, 615–627 (2011).
982 55. Moon, S. *et al.* A Robust Transposon-Endogenizing Response from Germline Stem Cells. *Dev. Cell* **47**,
983 660-671.e3 (2018).
984 56. Kang, I. *et al.* Identification of target genes regulated by the Drosophila histone methyltransferase
985 Eggless reveals a role of Decapentaplegic in apoptotic signaling. *Sci. Rep.* **8**, 7123 (2018).

986 57. Ota, R. & Kobayashi, S. Myc plays an important role in Drosophila P-M hybrid dysgenesis to eliminate
987 germline cells with genetic damage. *Commun. Biol.* **3**, 1–8 (2020).
988 58. Chu, H.-P. *et al.* Germline Quality Control: eEF2K Stands Guard to Eliminate Defective Oocytes. *Dev.*
989 *Cell* **28**, 561–572 (2014).
990 59. Chang, J. S., Tan, L. & Schedl, P. The *Drosophila* CPEB Homolog, Orb, Is Required for Oskar Protein
991 Expression in Oocytes. *Dev. Biol.* **215**, 91–106 (1999).
992 60. Ohtani, H. *et al.* DmGTSF1 is necessary for Piwi–piRISC-mediated transcriptional transposon silencing
993 in the Drosophila ovary. *Genes Dev.* **27**, 1656–1661 (2013).
994 61. Ji, S. *et al.* LC Domain-Mediated Coalescence Is Essential for Otu Enzymatic Activity to Extend
995 Drosophila Lifespan. *Mol. Cell* **74**, 363-377.e5 (2019).
996 62. Zhu, L., Kandasamy, S. K. & Fukunaga, R. Dicer partner protein tunes the length of miRNAs using
997 base-mismatch in the pre-miRNA stem. *Nucleic Acids Res.* **46**, 3726–3741 (2018).
998 63. Zhu, L., Liao, S. E. & Fukunaga, R. Drosophila Regnase-1 RNase is required for mRNA and miRNA
999 profile remodelling during larva-to-adult metamorphosis. *RNA Biol.* **16**, 1386–1400 (2019).
1000 64. Zhu, L., Kandasamy, S. K., Liao, S. E. & Fukunaga, R. LOTUS domain protein MARF1 binds CCR4-NOT
1001 deadenylase complex to post-transcriptionally regulate gene expression in oocytes. *Nat. Commun.* **9**,
1002 4031 (2018).
1003 65. Zhu, L. & Fukunaga, R. RNA-binding protein Maca is crucial for gigantic male fertility factor gene
1004 expression, spermatogenesis, and male fertility, in Drosophila. *PLOS Genet.* **17**, e1009655 (2021).
1005 66. Fukunaga, R. *et al.* Dicer Partner Proteins Tune the Length of Mature miRNAs in Flies and Mammals.
1006 *Cell* **151**, 533–546 (2012).
1007 67. Liao, S. E., Kandasamy, S. K., Zhu, L. & Fukunaga, R. DEAD-box RNA helicase Belle
1008 posttranscriptionally promotes gene expression in an ATPase activity-dependent manner. *RNA* **25**,
1009 825–839 (2019).

1010 68. Zhu, L., Liao, S. E., Ai, Y. & Fukunaga, R. RNA methyltransferase BCDIN3D is crucial for female fertility
1011 and miRNA and mRNA profiles in Drosophila ovaries. *PLOS ONE* **14**, e0217603 (2019).
1012 69. Rubin, T. & Huynh, J.-R. Mosaic Analysis in the Drosophila melanogaster Ovary. *Methods Mol. Biol.*
1013 *Clifton NJ* **1328**, 29–55 (2015).
1014 70. Kandasamy, S. K., Zhu, L. & Fukunaga, R. The C-terminal dsRNA-binding domain of Drosophila Dicer-2
1015 is crucial for efficient and high-fidelity production of siRNA and loading of siRNA to Argonaute2. *RNA*
1016 **23**, 1139–1153 (2017).
1017 71. Wang, L. *et al.* A Low-Cost Library Construction Protocol and Data Analysis Pipeline for Illumina-
1018 Based Strand-Specific Multiplex RNA-Seq. *PLOS ONE* **6**, e26426 (2011).
1019 72. Han, B. W., Wang, W., Li, C., Weng, Z. & Zamore, P. D. piRNA-guided transposon cleavage initiates
1020 Zucchini-dependent, phased piRNA production. *Science* **348**, 817–821 (2015).
1021 73. Zhang, Z., Theurkauf, W. E., Weng, Z. & Zamore, P. D. Strand-specific libraries for high throughput
1022 RNA sequencing (RNA-Seq) prepared without poly(A) selection. *Silence* **3**, 9 (2012).
1023

Figure 1. Azlan et al.

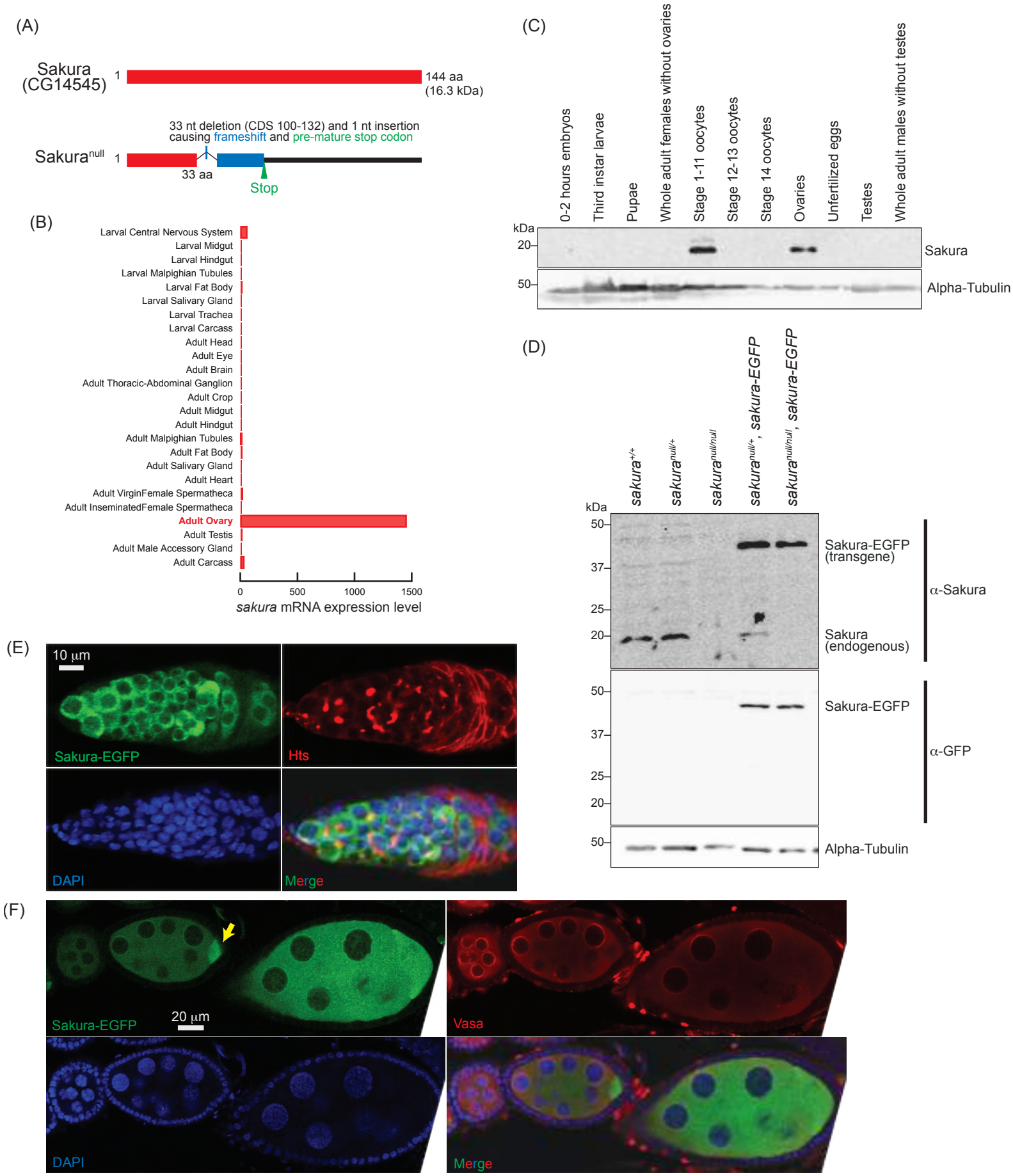

Figure 2. Azlan et al.

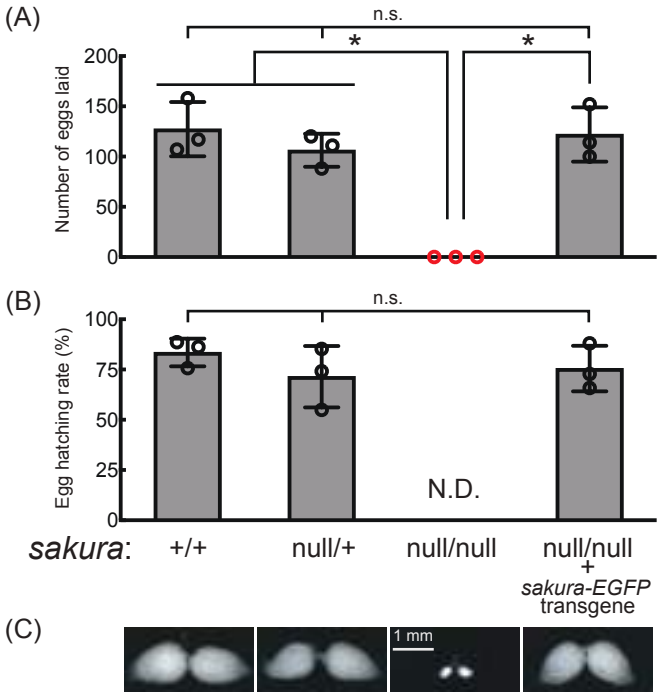

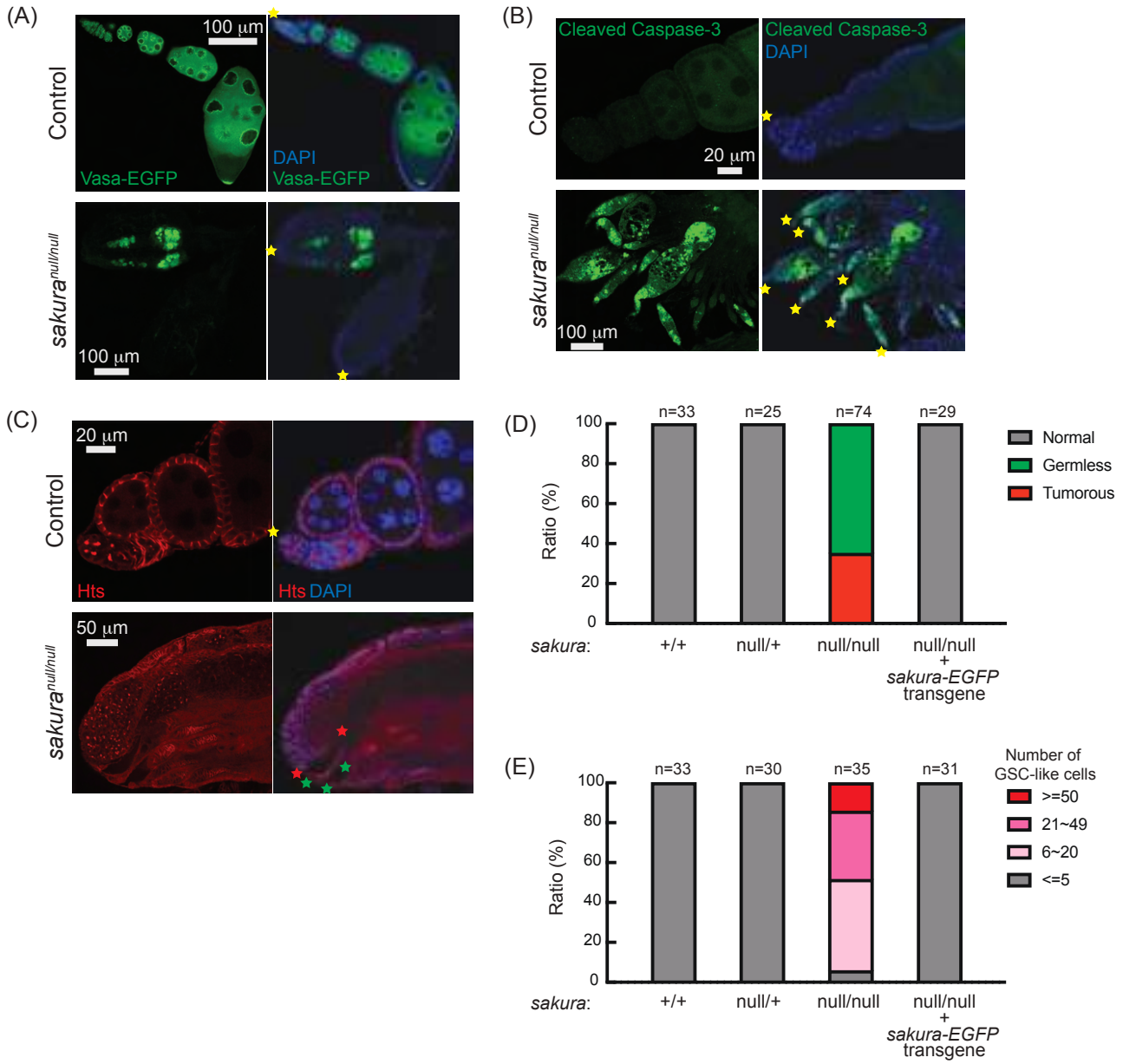
(A)
Control
100 μm
Vasa-EGFP
DAPI
Vasa-EGFP
sakura null/null
100 μm
(B)
Control
Cleaved Caspase-3
Cleaved Caspase-3
DAPI
20 μm
sakura null/null
100 μm
(C)
Control
20 μm
Hts
Hts DAPI
sakura null/null
50 μm
(D)
n=33
n=25
n=74
n=29
Ratio (%)
100
80
60
40
20
0
Normal
Germless
Tumorous
sakura:
+/+
null/+
null/null
null/null + sakura-EGFP transgene
(E)
n=33
n=30
n=35
n=31
Number of GSC-like cells
>=50
21~49
6~20
<=5
Ratio (%)
100
80
60
40
20
0
sakura:
+/+
null/+
null/null
null/null + sakura-EGFP transgene

(A) piRNA expression

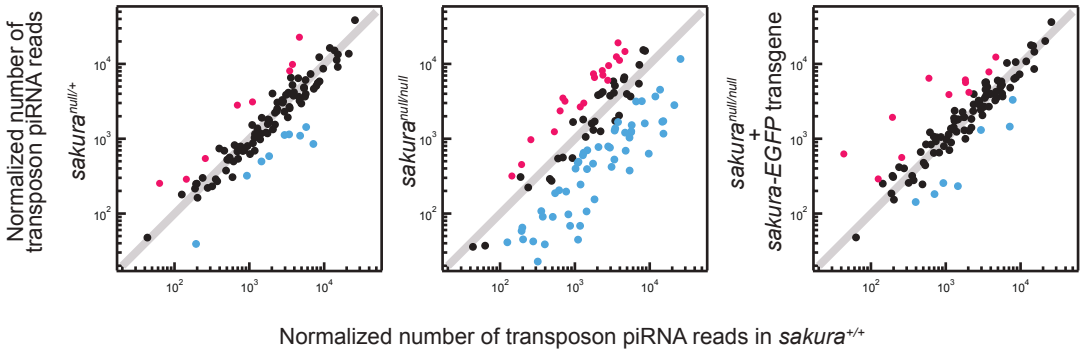

(B) Transposon RNA expression

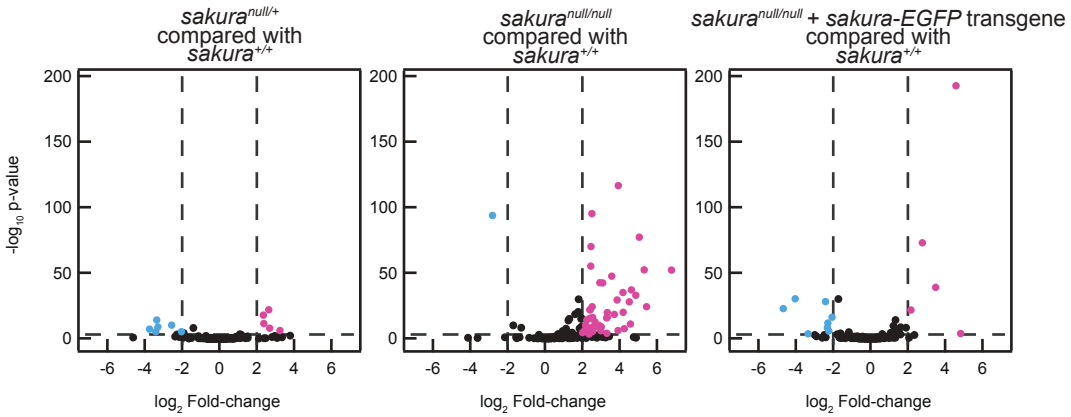

(C)

(D)

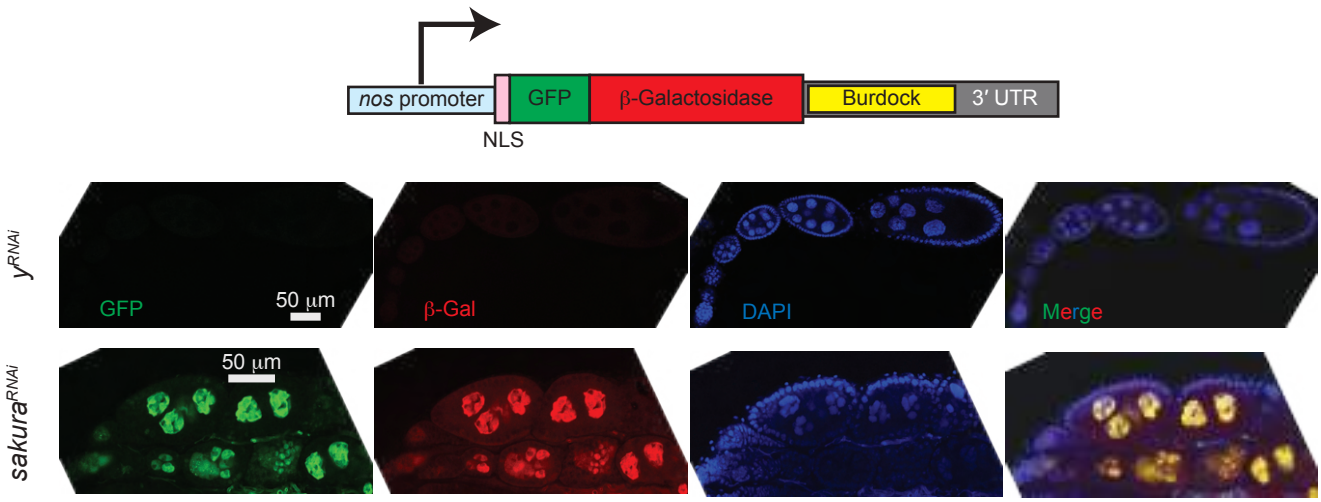

Figure 5. Azlan et al.

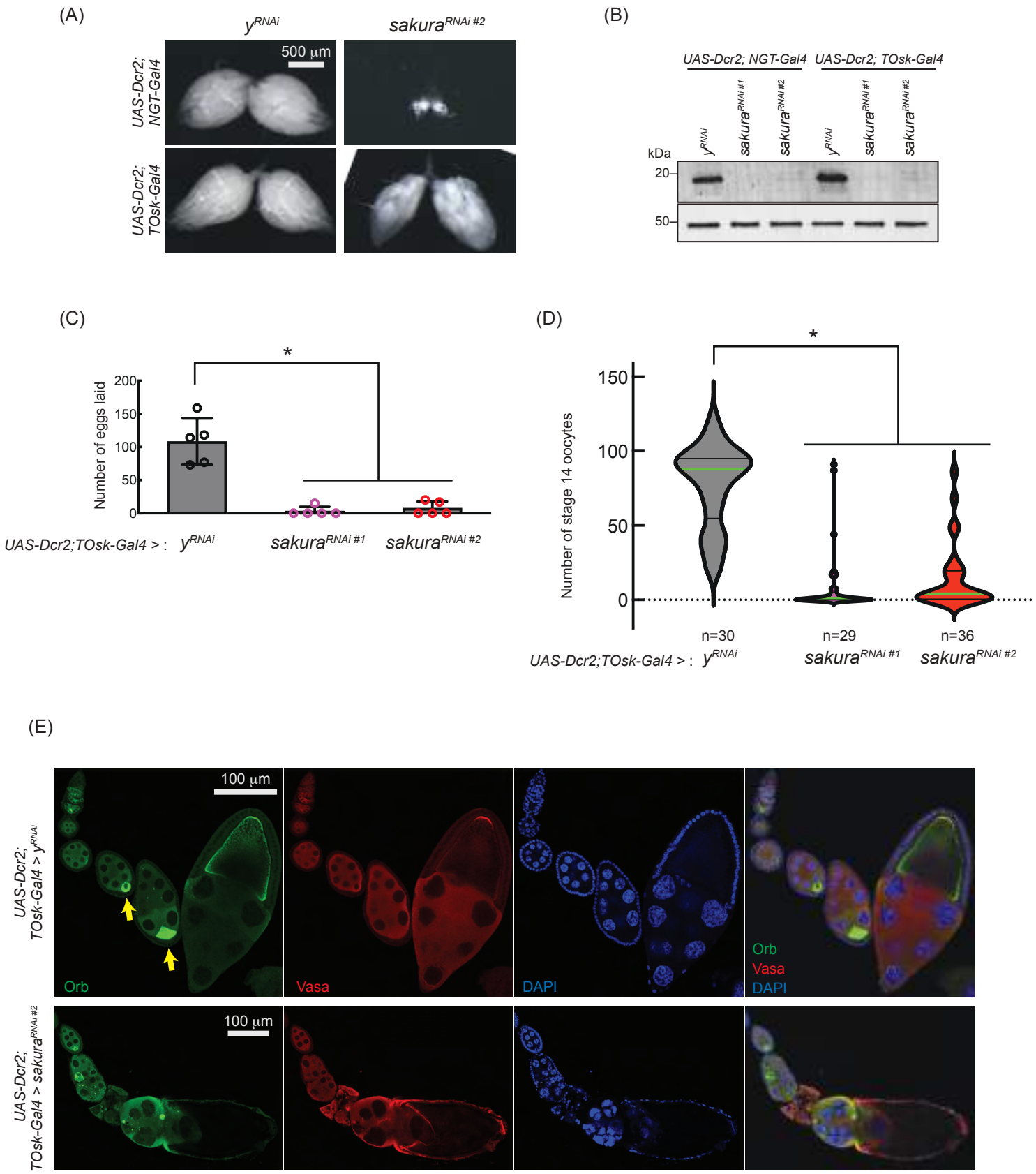

(A)

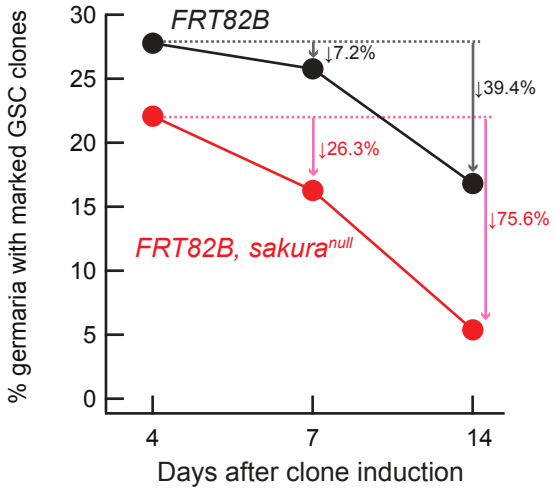

Genotype	Days after stopping heat shock	% marked GSCs	Relative % marked GSCs	Total number of germaria examined
hs-flp; +; *FRT82B, ubi-GFP / FRT82B* (control)	4	27.8	100	108
	7	25.8	92.8	97
	14	16.8	60.6	101
hs-flp; +; *FRT82B, ubi-GFP / FRT82B, sakura^null*	4	22.1	100	77
	7	16.3	73.7	86
	14	5.4	24.4	167

(B)

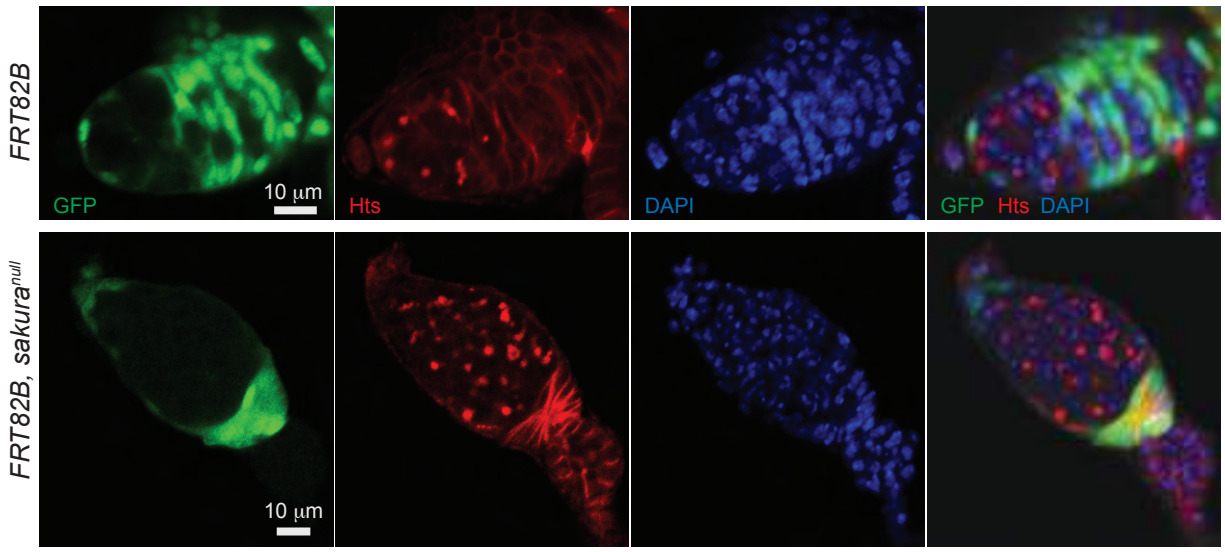

(C)

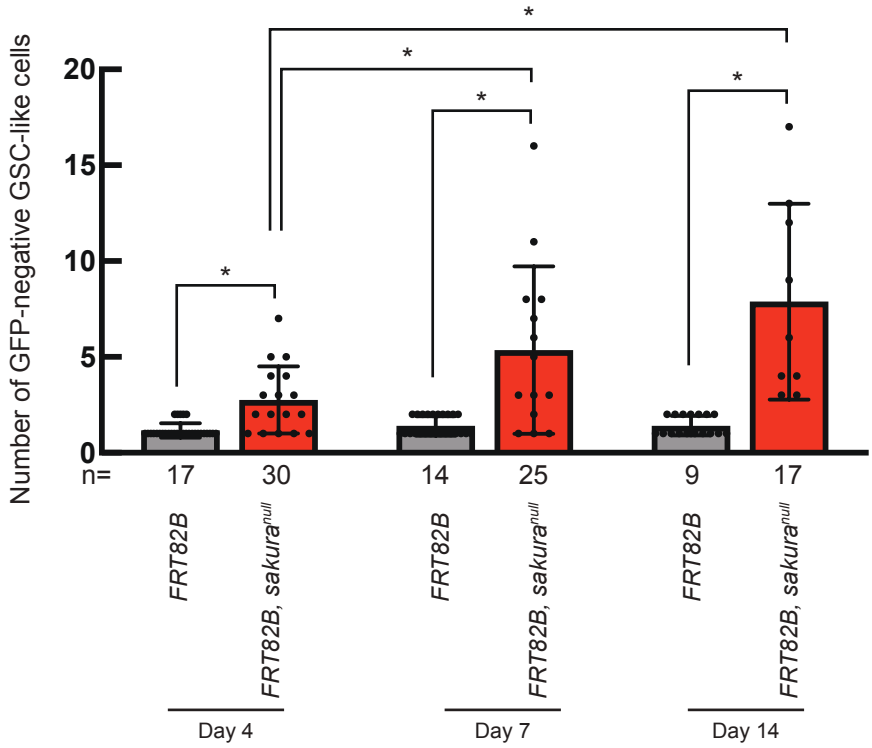

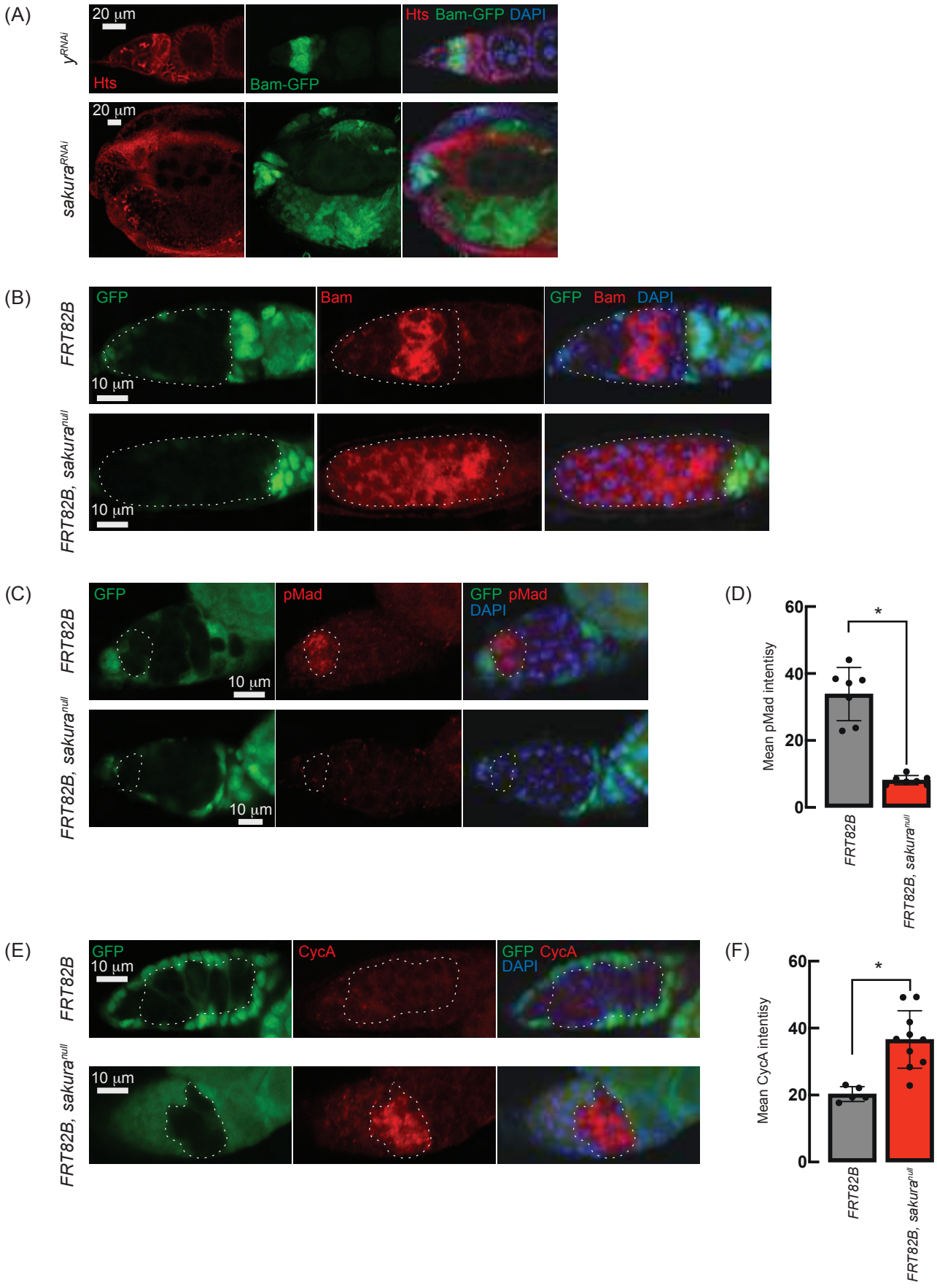
(A)
y^RNAi
sakura^RNAi
20 µm
Hts
Bam-GFP
Hts Bam-GFP DAPI
(B)
FRT82B
FRT82B, sakura^null
GFP
Bam
GFP Bam DAPI
10 µm
(C)
GFP
pMad
GFP pMad DAPI
(D)
Mean pMad intentisy
60
40
20
0
*
FRT82B
FRT82B, sakura^null
(E)
CycA
GFP CycA DAPI
(F)
Mean CycA intentisy

Figure 8. Azlan et al.

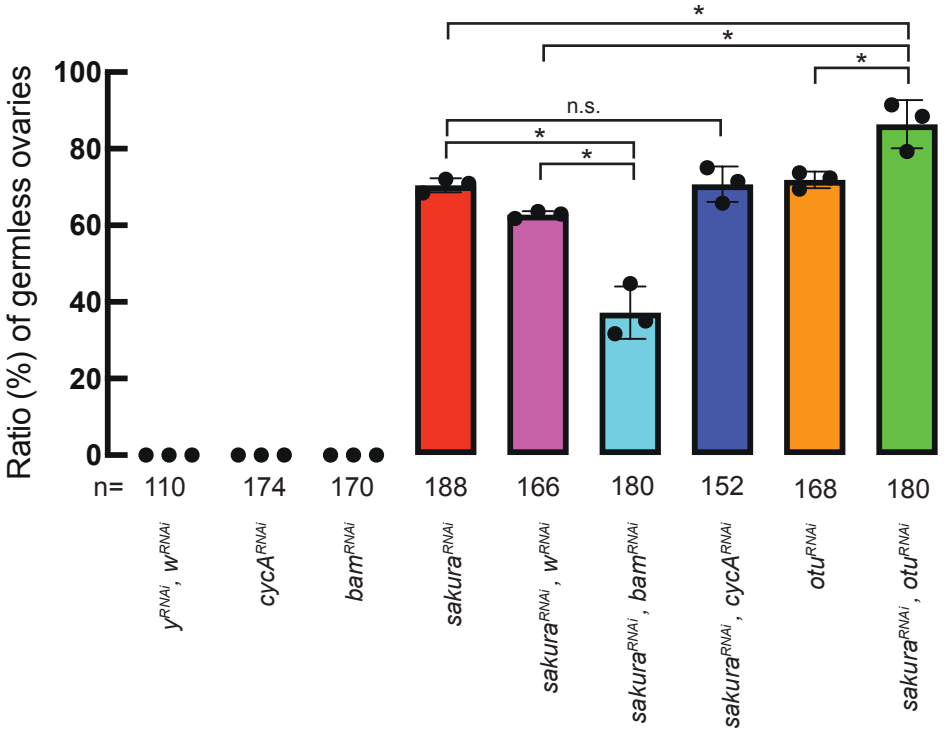

Figure 9. Azlan et al.

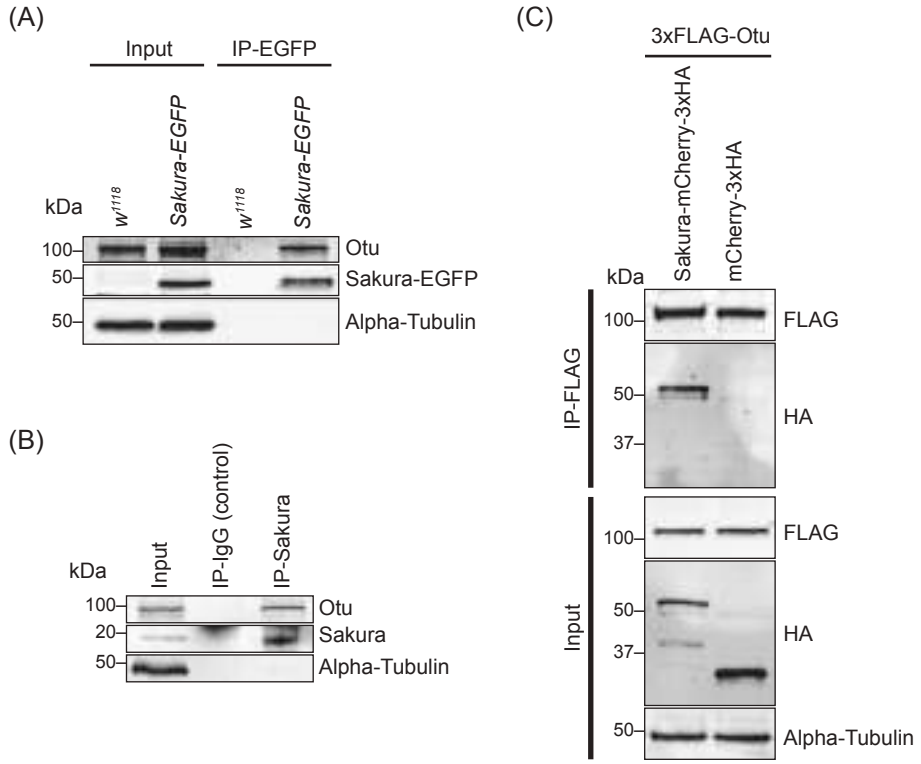

Figure 10. Azlan et al.

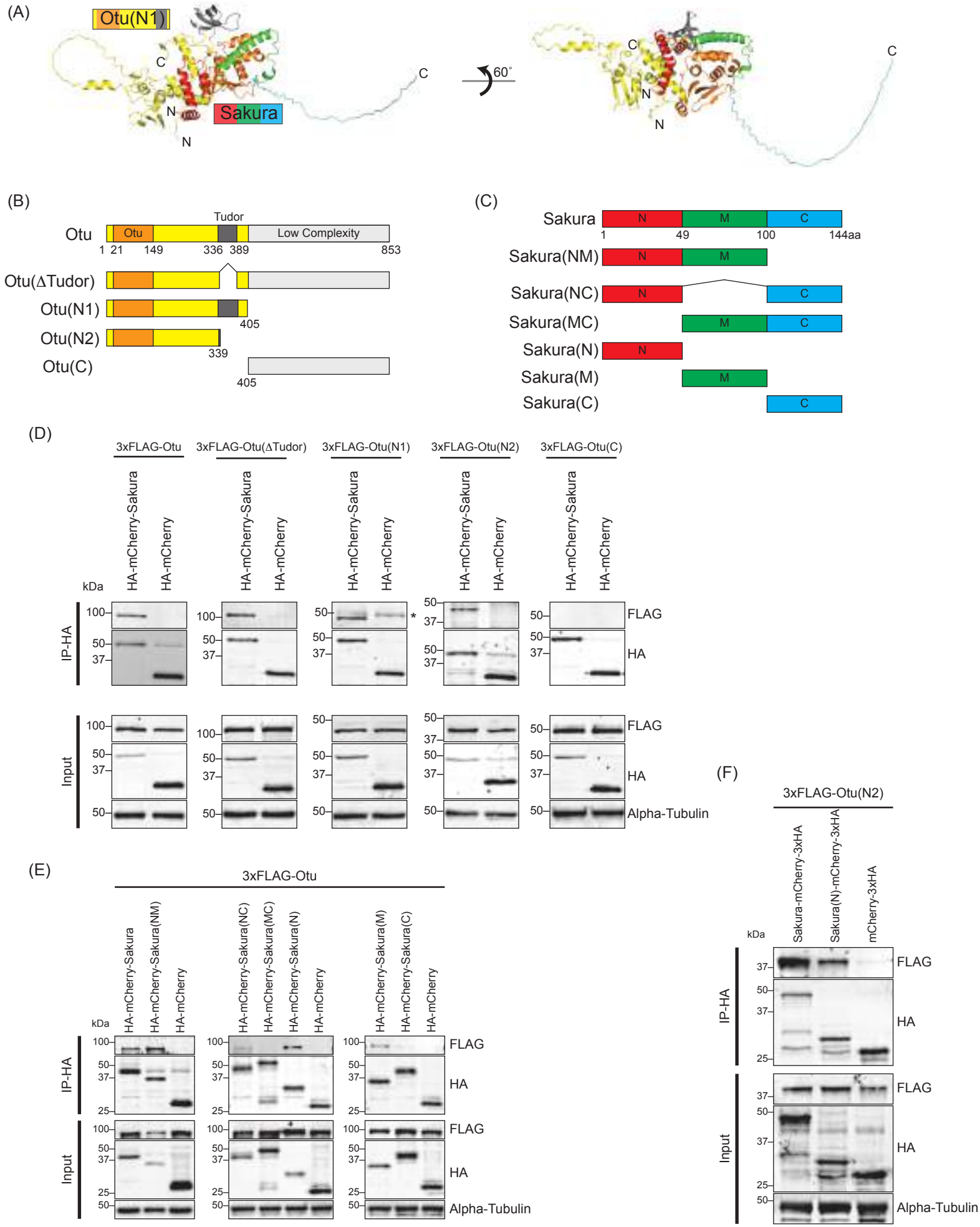

Figure 11. Azlan et al.

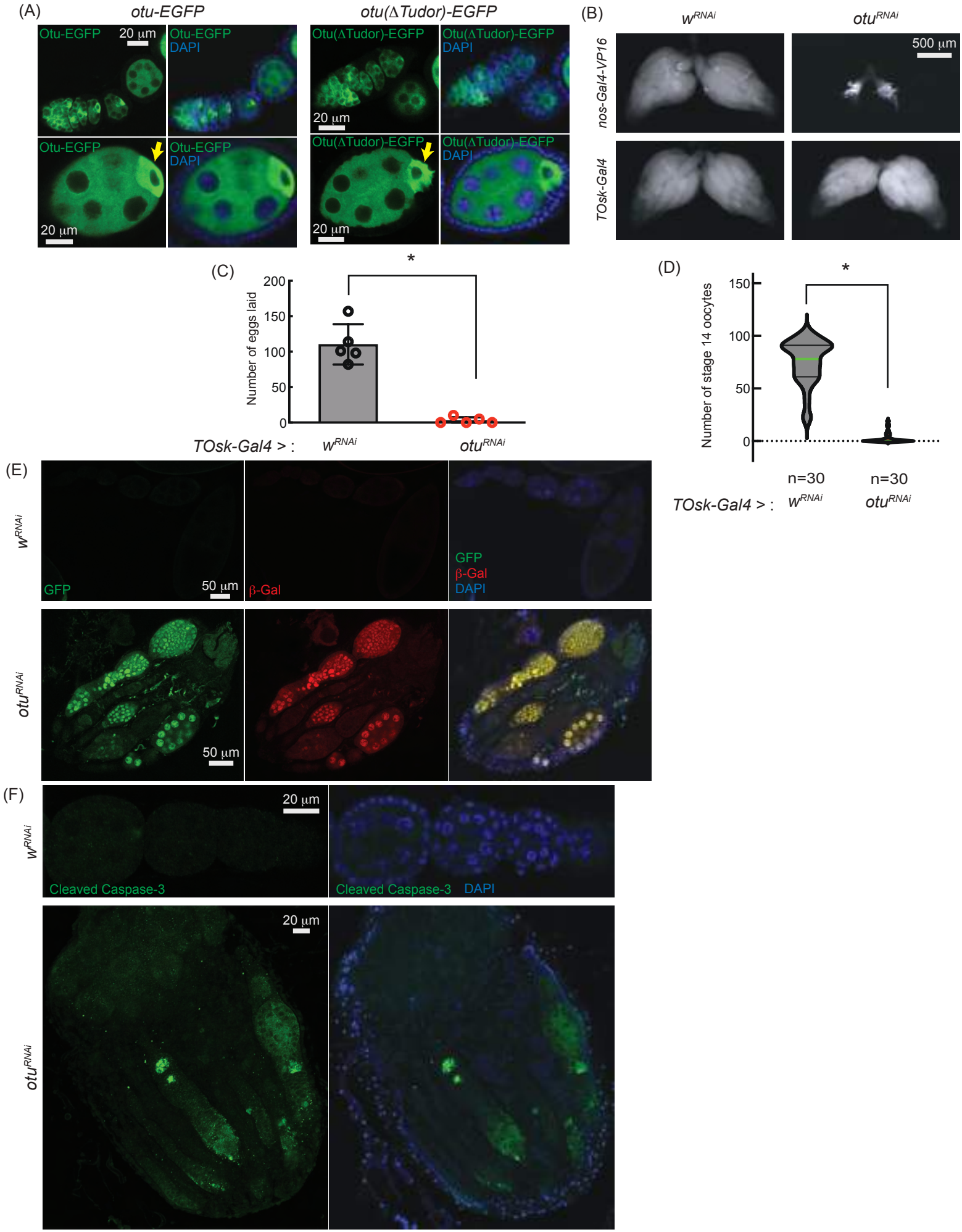

Figure 12. Azlan et al.

(A)

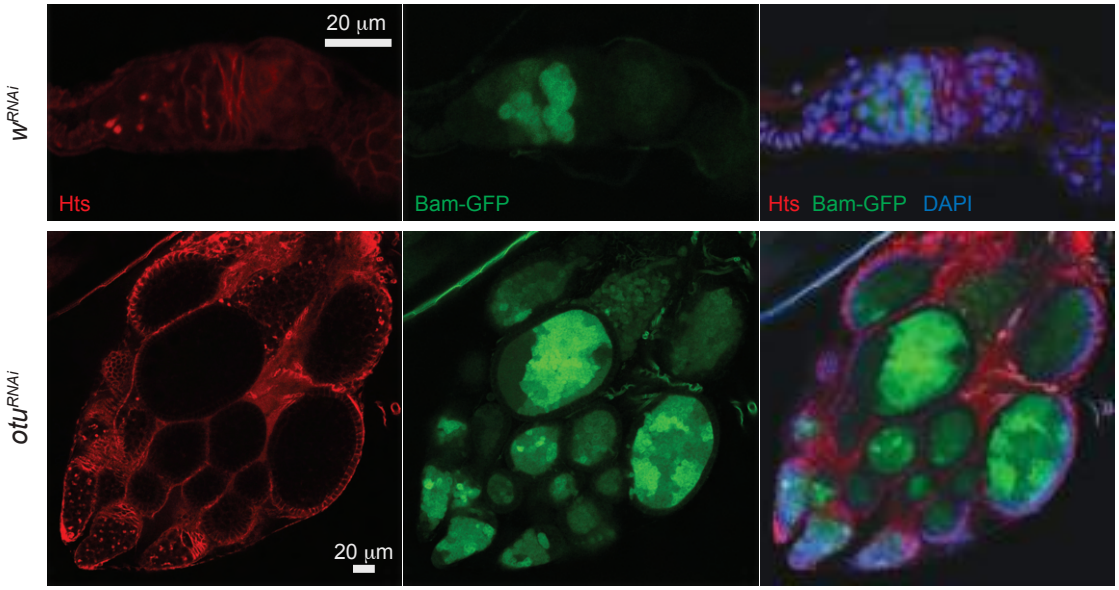

(B)

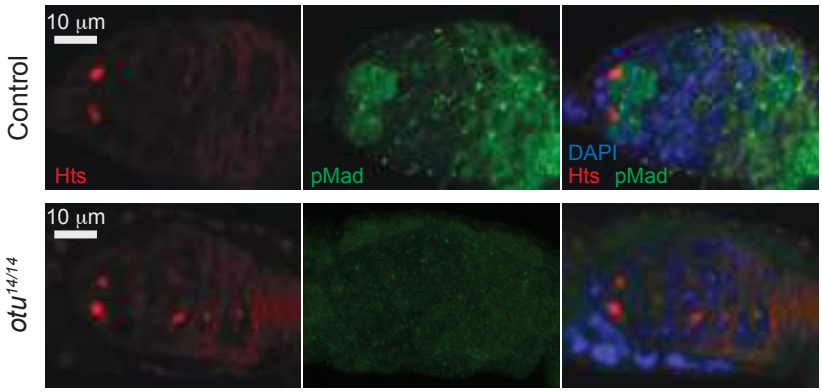

Figure S1. Azlan et al.

(A)

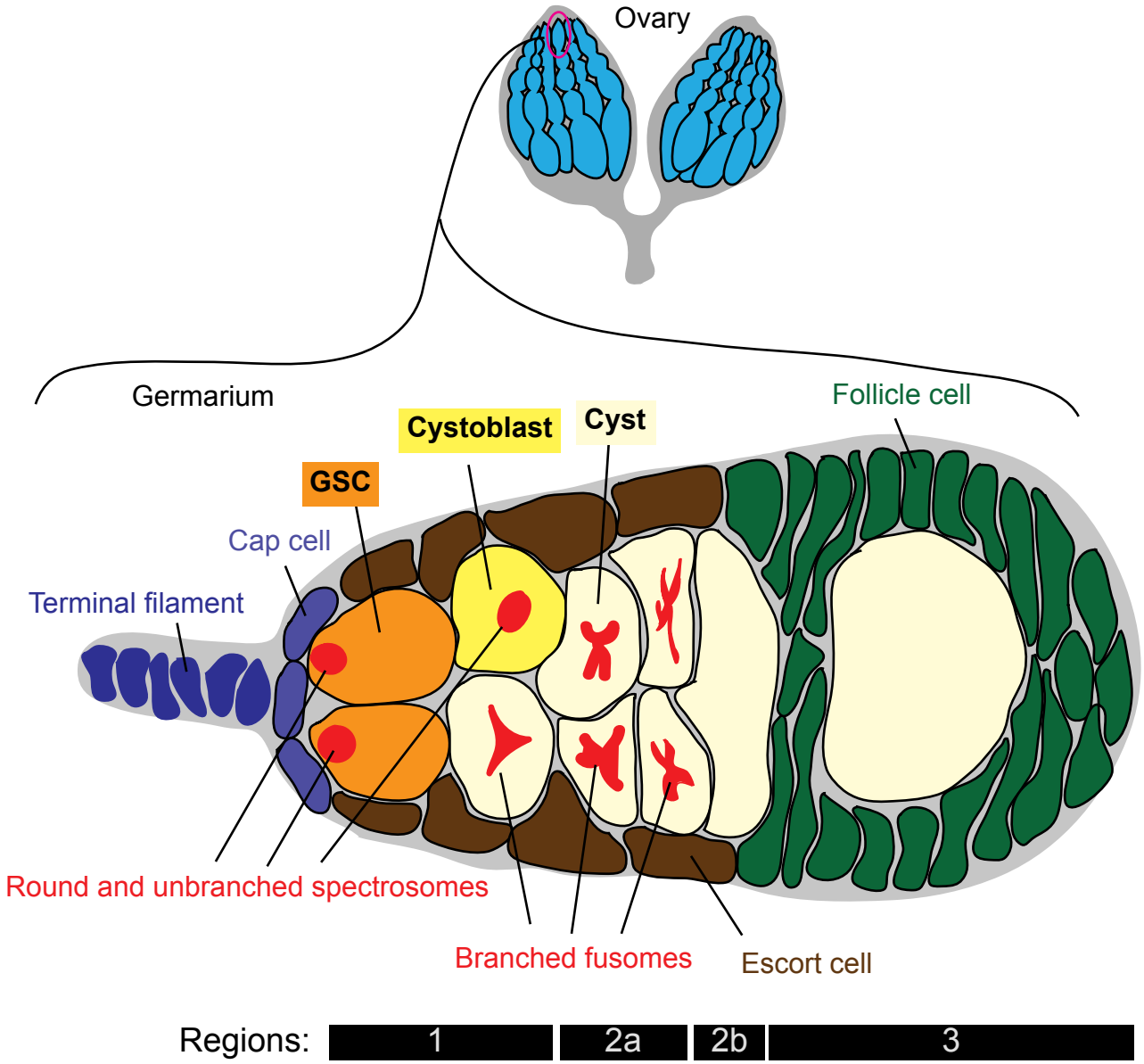

(B)

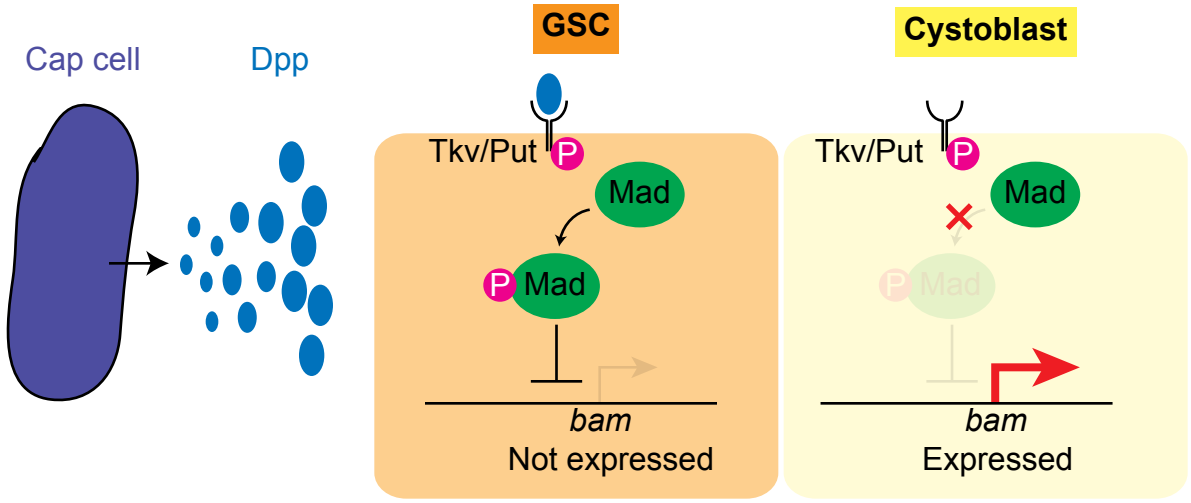

Figure S2. Azlan et al.

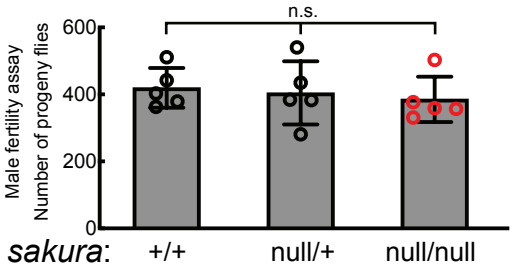

Figure S3. Azlan et al.

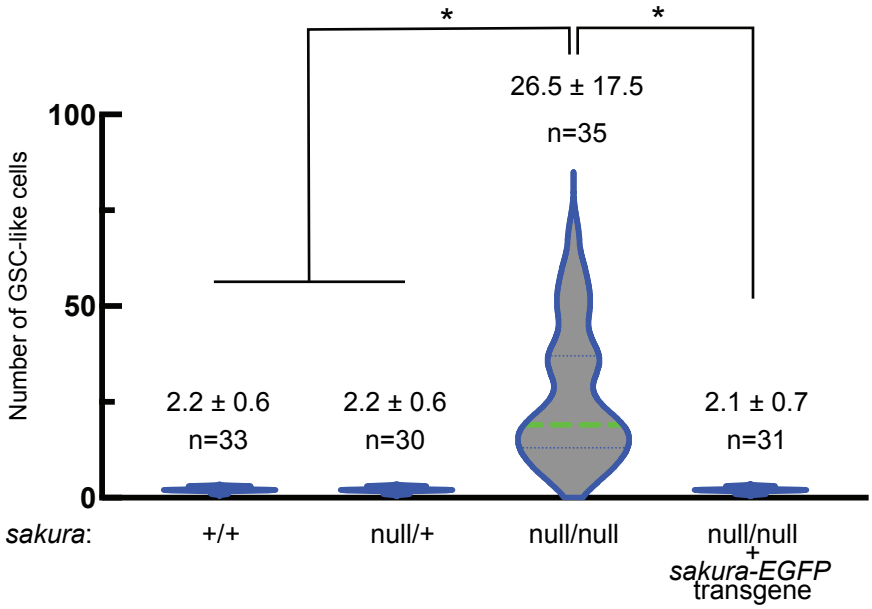

Figure S4. Azlan et al.

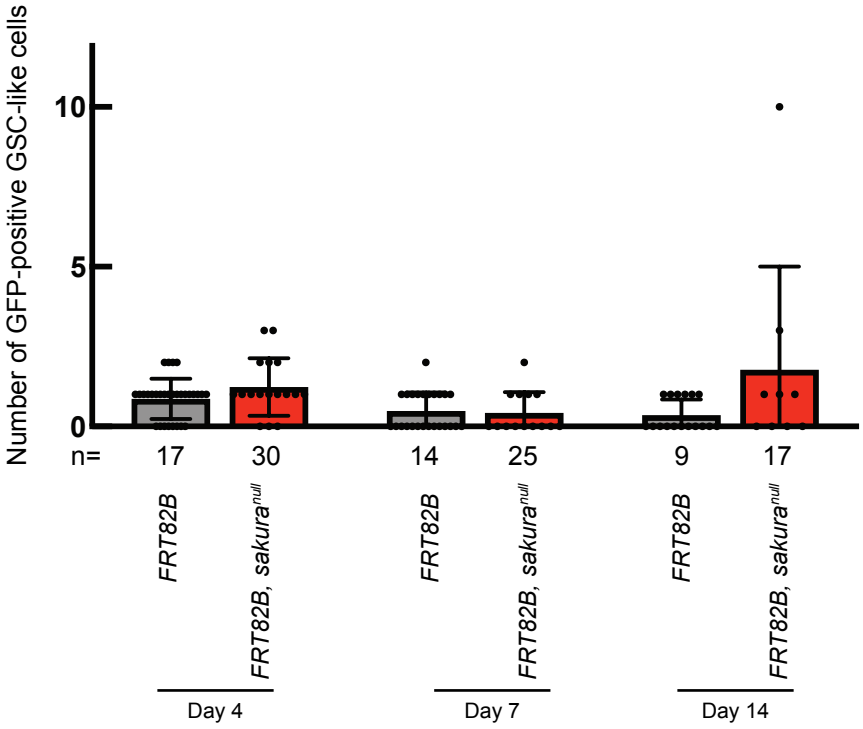

Figure S5. Azlan et al.

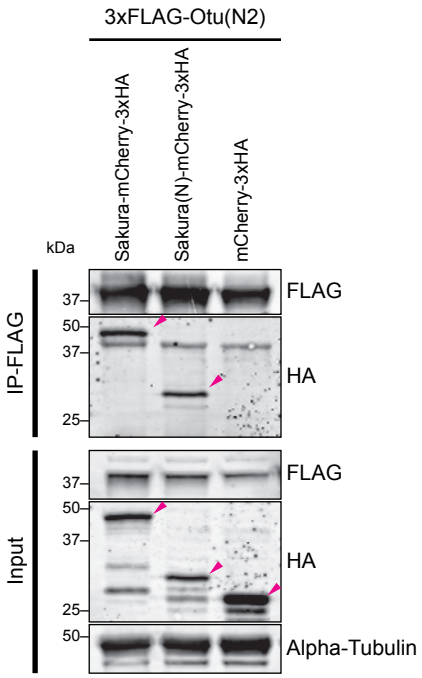
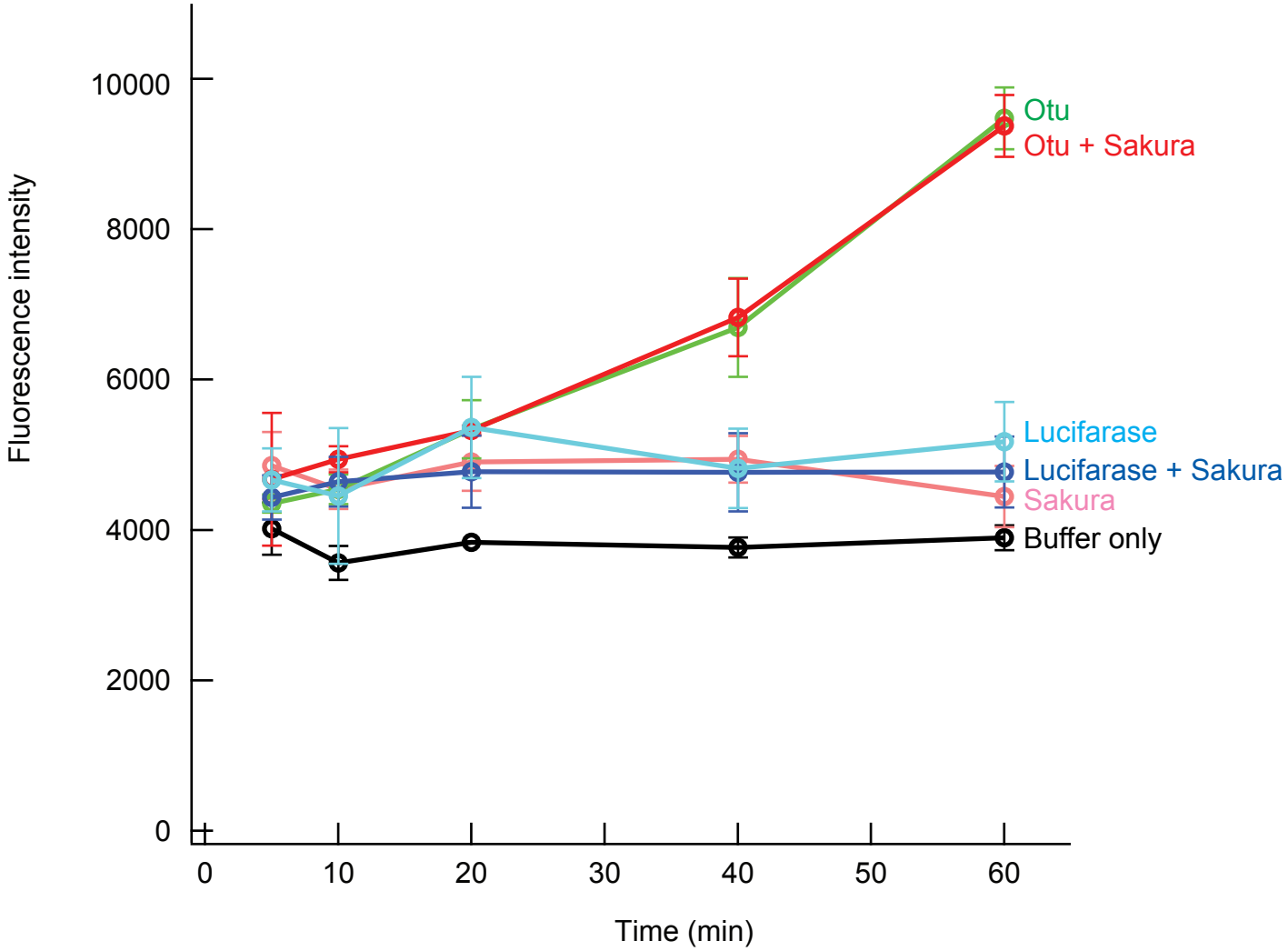
Figure S6. Azlan et al.